

Wave climate of the Hellenic Seas obtained from a wave hindcast for the period 1960–2001

Anna Zacharioudaki¹ · Gerasimos Korres² · Leonidas Perivoliotis²

Received: 26 September 2014 / Accepted: 21 April 2015 / Published online: 19 May 2015
© Springer-Verlag Berlin Heidelberg 2015

Abstract The wave climate of the Hellenic Seas and particularly the climate extremes are investigated by means of a 42-year (1960–2001) model hindcast. The wave model, implemented over the Mediterranean basin, is forced by high-resolution winds generated upon downscaling of the ERA40 reanalysis. It is shown that the quality of the hindcast is overall satisfactory; however, extreme wave heights in the Aegean Sea are consistently overestimated. Accordingly, corrections to the original data are applied. The results show that the highest mean wave conditions are located east and west of Crete Island where the northerly air flow exits the Aegean Sea. Extreme waves are the highest outside the Aegean Sea, mainly in the southern Ionian Sea and south of Crete. Nevertheless, high waves also develop around the exits of the Aegean Sea and N-NE of the Cyclades islands. Despite a milder extreme wave climate in the Aegean Sea due to short fetch distances, the mean wave height range is very similar to that of the Ionian Sea. Moreover, in summer, the two seas exhibit similar extreme wave height conditions with the highest extremes found around the exits of the Aegean Sea to the Levantine basin. Storms of a longer duration are also observed in the Aegean Sea. The analysis of long-term trends in the wave climate shows that mean and extreme wave

climate as well as the average intensity of extreme events have decreased in the Hellenic Seas. Nevertheless, this decrease has not been monotonic. A turning point is located around year 1981 with the mean and extreme wave height mostly increasing before this year and decreasing afterwards.

Keywords Waves · Wave climate · Climate extremes · Long-term changes · Climate variability · Hellenic Seas

1 Introduction

Knowledge of the wave climate is of paramount importance, especially within regions characterised by high offshore and coastal activity. Wave climate information, particularly on extreme events, is needed for the design and safety control of ships, offshore and coastal structures and touristic infrastructure. For coastal design, information on the prevailing wave conditions is equally important, since mean wave climate often drives long-term shoreline change, and is thus indispensable knowledge for coastal management. In recent years, when renewable energy production has become a priority in Europe, wave climate information is further needed for the design and safety control of wind and wave farms, but primarily, in the case of wave energy, for an assessment of the viability of such an option through resource characterisation. For long-term, sustainable planning of marine and coastal activities, the understanding of interannual variability and of climatic trends is also of great importance, especially in the context of climate change. Historic and future wave climate changes may require adaptation measures.

In the past, regional to global scale wave climate studies, were based on voluntary observing ship wave data. These data however are of poor sampling density and are particularly limited during extreme conditions (e.g. Gulev et al. 2003).

Responsible Editor: Birgit Andrea Klein

✉ Anna Zacharioudaki
azacharioudaki@hcmr.gr

¹ Hellenic Centre for Marine Research, Institute of Oceanography, Former US Base at Goumes, P.O. Box 2214, 71003 Heraklion, Crete, Greece

² Hellenic Centre for Marine Research, Institute of Oceanography, 46.7 km Athens-Sounio Ave., P.O. Box 712, 19013 Anavyssos, Attiki, Greece

Towards the end of the 1990s, the advance of numerical wave models together with the increase in computational power brought about wave climate studies based on numerical wave hindcast (e.g. WASA Group 1998). At present, this approach is the most suitable for wave climate investigations because it allows for the production of long-term, as homogeneous as possible (data assimilation may change the quality of the dataset over a long time period) and uninterrupted wave datasets with a good spatial and temporal resolution. In situ and satellite wave recordings are used to validate the numerical models but may not be used on their own for medium- to large-scale wave climate studies because of poor spatial and/or temporal resolution, data inhomogeneities and gaps and short duration datasets at present.

Several studies exist on the wave climate of the Mediterranean Sea (e.g. Lionello and Sanna 2005; Musić and Nicković 2008; Ratsimandresy et al. 2008). From those, a few cover or partly cover the Hellenic Seas, i.e. the area of interest in this study. Athanassoulis and Skarsoulis (1992) produced a wind and wave atlas of the Northeastern Mediterranean Sea, presented on a $1 \times 1^\circ$ grid and based on visual observations (1850–1980). In 2004, a wind and wave atlas of the entire Mediterranean Sea, commissioned by the Italian, French and Greek navies, was completed by the Medatlas Group (2004). Buoy, satellite and numerical model data, spanning a period of 10 years, were combined to produce results both on mean and severe wave conditions. Similarly, Soukissian et al. (2008) used a 10-year wave hindcast to examine wave climatology in the Hellenic Seas. Lionello and Sanna (2005), using a 44-year wave hindcast forced by coarse resolution winds (over 100 km), examined mean wave height variability in the Mediterranean Sea. The latter was also studied by Queffeulou and Bentamy (2007) but with the sole use of satellite measurements over a 14-year period. Finally, Musić and Nicković (2008) presented results on the wave interannual variability and climatic trends of different wave height percentiles at 31 points in the Eastern Mediterranean. The study used a 44-year wave hindcast forced by high-resolution winds.

From the above studies, those based on visual observations or satellite data suffer from the problems associated with such datasets, mentioned earlier. Those who used datasets shorter than 15 years take into account only a small part of the interannual variability and do not allow for the estimation of trends. Studies which employed coarse resolution wind and/or wave models are unable to resolve the highly variable wind and wave fields of the Hellenic Seas, caused by the presence of a pronounced orography and of numerous islands creating both sheltering and channelling effects. Systematic underestimation of the simulated variables has been associated with these studies (e.g. Cavaleri and Bertotti 2004). Consequently, they may infer mean climatic variability and trends but they may not assess extreme values. In fact, only

the study by Musić and Nicković (2008) fulfilled the requirements for a thorough wave climate assessment in the Mediterranean. Nevertheless, this study produced output only at selected locations giving no estimates of the significance of the presented trends and omitting seasonality.

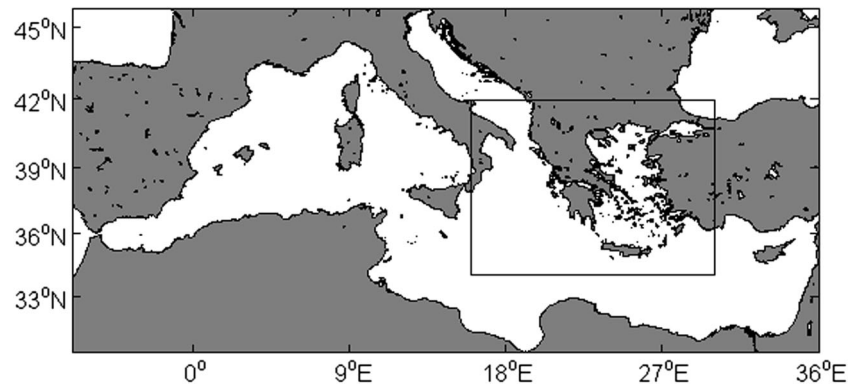
The present study generates a 42-year wave hindcast at a spatial resolution of 0.1° , forced by wind fields at a resolution of 0.5° , in an attempt to assess the wave climate of the Hellenic Seas. Following studies like that of Weisse and Günther (2007) or of Appendini et al (2014) on the wave climate of the Southern North Sea and of the Gulf of Mexico, respectively, the present study goes a step further than the existing studies on the wave climate of the Mediterranean Sea mentioned above and includes the estimation of parameters important for engineering applications such as significant wave height return periods and storm characteristics namely storm duration and intensity. The authors believe that this is a crucial task for the Hellenic Seas as this region is characterised by the largest merchant fleet in the EU—and one of the largest fleets in the world—and has a highly developed coastal touristic infrastructure. The Aegean and Ionian Seas surrounding Greece constitute one of the main links of Europe to the Eastern Mediterranean and Russia. Therefore, these areas serve as the main routes of oil transportation from source to Europe. This results in a continuous pressure on the marine environment. Additionally, and after completing seismic explorations, the areas south of Crete and the eastern Ionian have been recently proposed as a potentially significant reservoir of oil and gas. If this is proven, intensified offshore oil and gas extraction is expected to begin in the near future.

The outline of this paper is as follows: The model setup is described in Sect. 2. In Sect. 3, the wave model output is validated against observations and, with a focus on extremes, corrections are applied to the original hindcast. Section 4 presents the wave climate of the Hellenic Seas whilst Sect. 5 gives estimates of wave height return levels. Section 6 focuses on wave climate trends. The main conclusions from this work are outlined in Sect. 7.

2 Model setup

The WAM (cycle 4) model (WAMDI Group 1988), a third-generation wave model that explicitly solves the wave transport equation, was used to perform the wave hindcast for this study. This is a widely used model that has been extensively validated by the scientific community. It has been applied by Korres et al. (2011) in the Mediterranean Sea, and its performance has been intercompared with the WW3 model. WAM is also a forecasting component of the POSEIDON monitoring and forecasting system (Nittis et al. 2010) used to issue wave forecasts for the Mediterranean and the Aegean Seas. In the model, the wind input, non-linear energy transfer and white

Fig. 1 WAM model domain. The internal rectangle corresponds to the Hellenic Seas



capping dissipation source terms are explicitly prescribed and integrated using an implicit second-order-centred differencing scheme. For the propagation term, a first-order upwind scheme is applied. More details on the model can be found in WAMDI Group (1988) or Günther et al. (1992).

For this study, the WAM was implemented in the Mediterranean Sea (-7° W to 36° E, 30.25° N to 45.75° N) with a spatial resolution of 0.1° (Fig. 1), spherical propagation and deep water conditions. The spectral discretisation comprised 30 frequencies and 24 directions whilst the wave

propagation time step was set to 300 s. The ETOPO2 bathymetric dataset at 2-min resolution (NGDC 2006) was used to setup the model bathymetry. The wind forcing originated from the ARPERA wind hindcast (Herrmann and Somot 2008; Martínez-Asensio et al. 2013), a dynamical downscaling of the global ERA-40 reanalysis (Uppala et al. 2005). This hindcast provided 10-m winds with a spatial resolution of ~ 50 km and a temporal resolution of 6 h for the period 1960–2001. Following the empirical method described in Ruti et al (2008) corrections to the original ARPERA wind

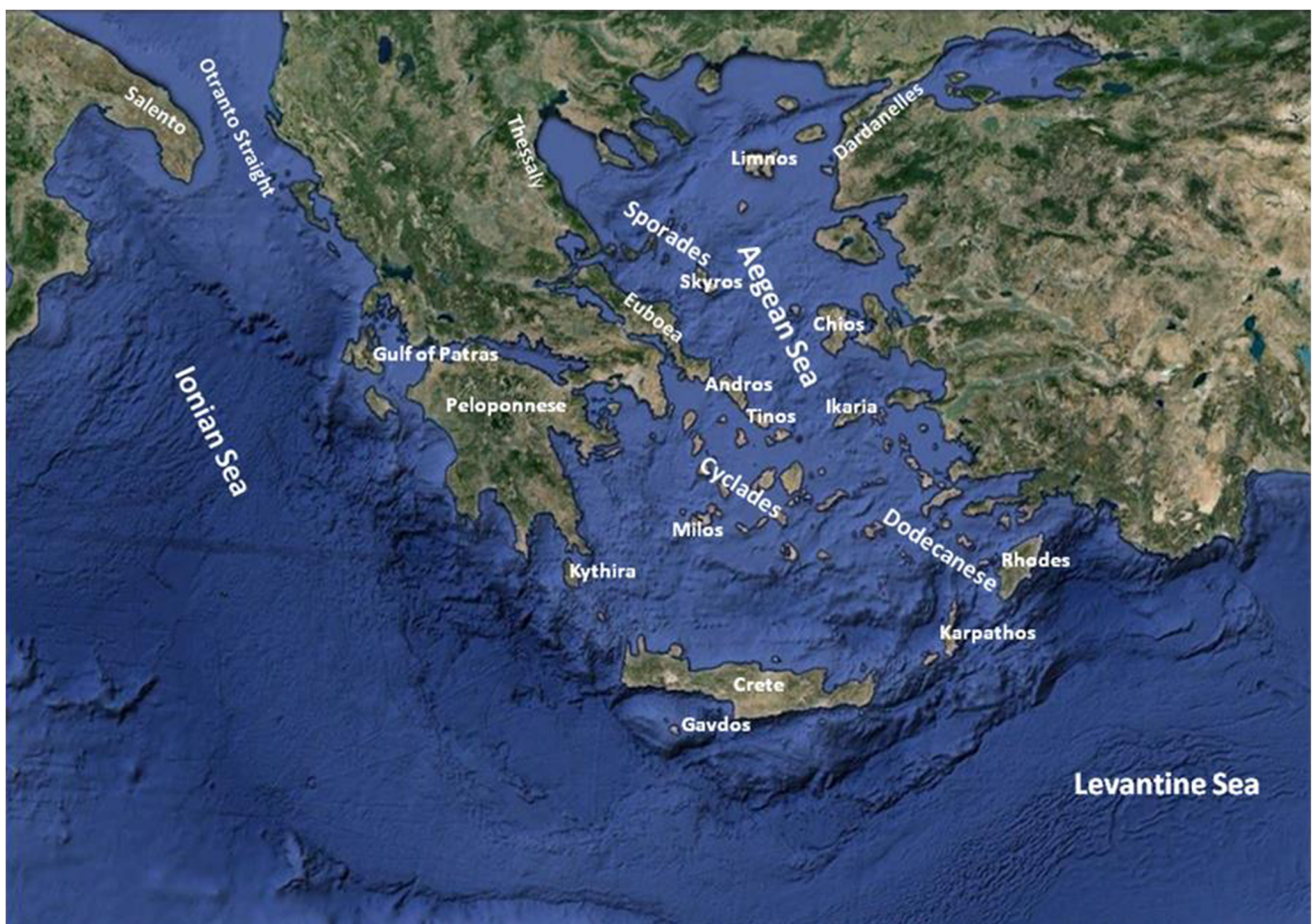
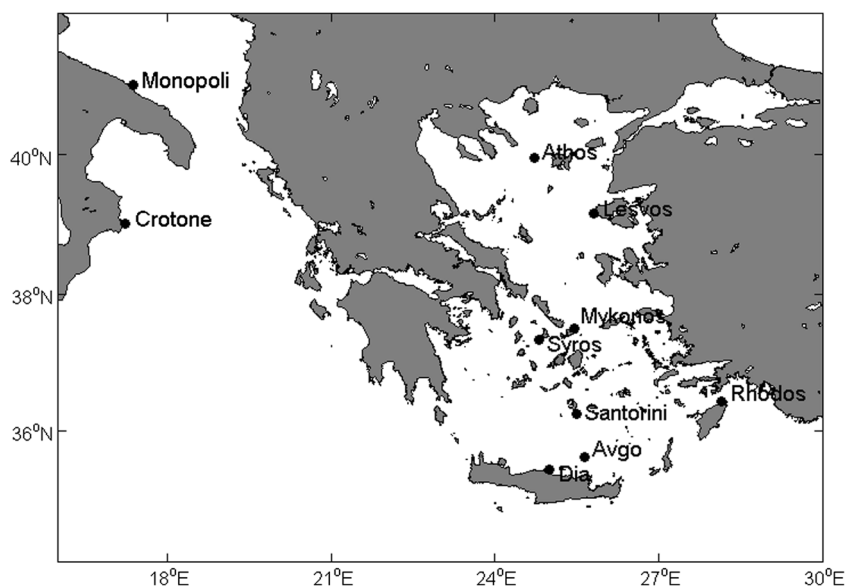


Fig. 2 Geography of the Hellenic Seas

Fig. 3 Wave buoys' location

speeds were applied by Krokos and Korres (2010) using QuikSCAT scatterometer wind fields. Specifically, linear regression was used to adjust the slope of the original ARPERA wind speeds over each overlapping ARPERA-QuikSCAT grid point and for the overlapping period 1999–2001. QuikSCAT wind speed values less than 5 m/s were omitted from the analysis as these were found to be overestimated by the scatterometer. Slopes were adjusted separately for winter and summer, and the corrections were extended over the whole 1960–2001 period. The corrected winds fields were used herein to drive WAM over the coincident 42-year period (1960–2001) producing wave parameters at six-hourly intervals.

In this paper, the focus is on the Hellenic Seas from 16° E to 30° E and from 34.05° N to 41.95° N (Fig. 1). Thus, the wave

hindcast validation and the results presented below concern only this region. The geography of the examined domain is shown in Fig. 2.

3 Validation/calibration of the wave hindcast

3.1 Validation

The extent to which the wave hindcast reproduced observed conditions in the Hellenic Seas was investigated through its comparison with in situ measurements as well as with satellite data. The in situ measurements used for the validation of the wave hindcast came from eight wave buoys of the POSEIDON network, managed by HCMR (Greece), and

Table 1 Buoy stations with location and water depth

| Station | Buoys | | Closest grid point | |
|-----------|-----------------|-----------|--------------------|---------------|
| | Location (°) | Depth (m) | Location (°) | Distance (km) |
| Athos | 39.96 N 24.72 E | 212 | 39.95N 24.7 E | 2.5 |
| Lesvos | 39.15 N 25.81 E | 121 | 39.15 N 25.8 E | 1.04 |
| Mykonos | 37.51 N 25.45 E | 138 | 37.55N 25.5 E | 5.95 |
| Syros | 37.35 N 24.80 E | 87 | 37.35 N 24.8 E | 0 |
| Rhodes | 36.45 N 28.15 E | 233 | 36.45 N 28.1 E | 4.6 |
| Santorini | 36.25 N 25.49 N | 314 | 36.25 N 25.5 E | 1.23 |
| Avgo | 35.62 N 25.64 E | 354 | 35.65 N 25.6 E | 5.2 |
| Dia | 35.44 N 25.14 E | 320 | 35.45 N 25.1 E | 9.5 |
| Crotone | 39.00 N 17.22 E | 80 | 38.95 N 17.2 E | 8.3 |
| Monopoli | 40.97 N 17.38 E | 85 | 40.95 N 17.4 E | 3.46 |

The location and distance to the closest grid point is also listed

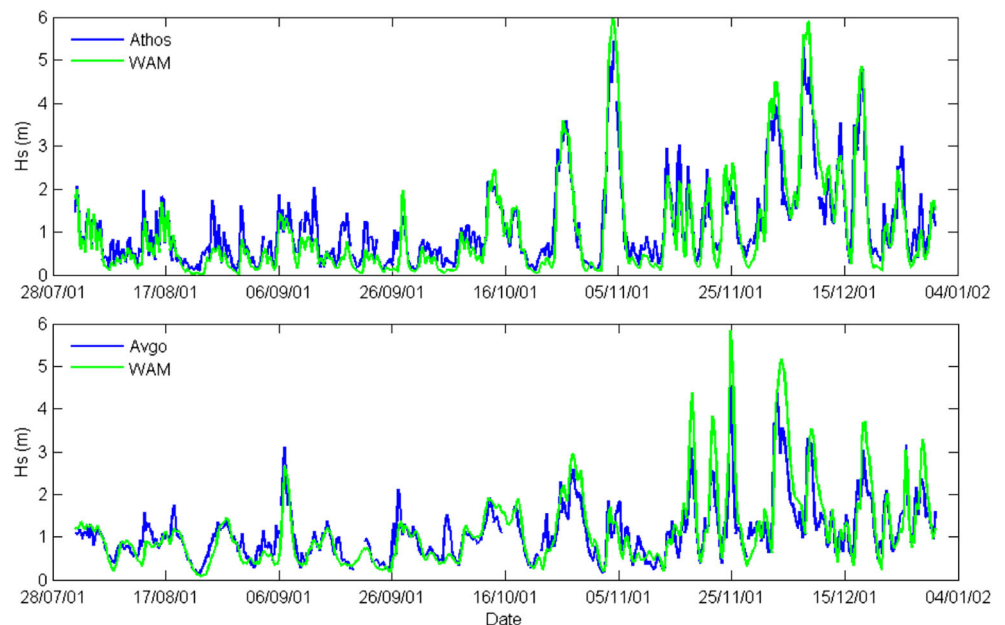
Table 2 Statistical parameters of the comparison between the model hindcast SWH and in situ measurements at different wave buoy locations

| | | Athos | Lesvos | Mykonos | Syros | Rhodes | Santorini | Avgo | Dia | Crotone | Monopoli |
|-----------------------------------|---------------------------------|-------|--------|---------|-------|--------|-----------|-------|-------|---------|----------|
| All H_s | N | 1932 | 2814 | 2558 | 812 | 1299 | 3090 | 2294 | 1379 | 16,895 | 17,157 |
| | R | 0.93 | 0.89 | 0.89 | 0.92 | 0.78 | 0.84 | 0.9 | 0.89 | 0.92 | 0.86 |
| | \bar{X}_{obs} (m) | 0.82 | 0.81 | 1.07 | 0.78 | 0.54 | 0.9 | 0.99 | 0.89 | 0.73 | 0.68 |
| | $\bar{X}_{\text{hindcast}}$ (m) | 0.67 | 0.85 | 1.04 | 0.85 | 0.61 | 1 | 0.99 | 0.84 | 0.72 | 0.59 |
| | Relative Bias | 0.18 | -0.05 | 0.03 | -0.08 | -0.14 | -0.11 | 0 | 0.06 | 0.02 | 0.13 |
| | RMSE (m) | 0.35 | 0.38 | 0.41 | 0.34 | 0.34 | 0.46 | 0.34 | 0.37 | 0.29 | 0.32 |
| | Scatter Index | 0.42 | 0.46 | 0.38 | 0.43 | 0.62 | 0.51 | 0.34 | 0.42 | 0.39 | 0.46 |
| $H_s \geq 90\text{th percentile}$ | N | 193 | 281 | 256 | 81 | 130 | 309 | 229 | 138 | 1917 | 2055 |
| | R | 0.87 | 0.67 | 0.7 | 0.54 | 0.6 | 0.3 | 0.7 | 0.66 | 0.77 | 0.7 |
| | \bar{X}_{obs} | 2.62 | 2.15 | 2.79 | 2.03 | 1.14 | 2.21 | 2.39 | 2.3 | 2.1 | 1.81 |
| | $\bar{X}_{\text{hindcast}}$ | 2.57 | 2.38 | 2.8 | 2.42 | 1.53 | 2.51 | 2.57 | 2.57 | 2.16 | 1.75 |
| | Relative Bias | 0.02 | -0.11 | 0 | -0.19 | -0.34 | -0.14 | -0.08 | -0.12 | -0.03 | 0.03 |
| | RMSE | 0.63 | 0.67 | 0.64 | 0.65 | 0.68 | 0.93 | 0.72 | 0.74 | 0.57 | 0.58 |
| | Scatter Index | 0.24 | 0.31 | 0.23 | 0.32 | 0.6 | 0.42 | 0.3 | 0.32 | 0.27 | 0.32 |

two wave buoys of the Italian Data Buoy Network (RON), managed by ISPRA (Italy). The buoys' location and name are shown in Fig. 3. A list of their coordinates and water depth is given in Table 1 together with the corresponding coordinates and distance to the closest model grid point used for the comparisons. POSEIDON data begin on June 1999, thus, the overlapping period with the wave hindcast was up to 2.5 years whilst RON data begin in 1989 with the overlapping period reaching 12 years. Coincident in time model output and buoy measurements were selected for the validation. The satellite data used for the validation were obtained from a merged altimeter wave height database setup at IFREMER (France).

This database contains altimeter data that begin in 1991 and that have been filtered and corrected (Queffelec and Croizé-Fillon 2013). Here, data from four satellite missions, the ERS1 (1991–1996), ERS2 (1995–2001), TOPEX POSEIDON (1992–2001) and GEOSAT FO (2000–2001), were used. To collocate model output and satellite data the former were interpolated in time and space to the individual satellite tracks. For each track, corresponding to one satellite pass, along-track pairs of satellite data and interpolated model output were brought to the nearest wind model grid point (0.5°) and those pairs on the same grid point were averaged.

Fig. 4 Time-series of SWH at Athos and Avgo for the period 1 Aug 01–31 Dec 01; observations (blue line) versus WAM output (green line)



Statistical parameters of the comparison between the model hindcast significant wave height (SWH) and the measured SWH at the different wave buoy locations (Fig. 3) are presented in Table 2. In the Table, H_s is the SWH, n is the number of collocated data available for the estimation of each statistical measure whilst \bar{X}_{obs} and $\bar{X}_{\text{hindcast}}$ represent the mean value of the observations and the hindcast respectively. Also shown are the Pearson correlation coefficient (R), the *relative bias*, the root mean square error (RMSE) and the *scatter index* which are statistics that are commonly applied to assess numerical model skill (e.g. Musić and Nicković 2008). The relative bias is defined as the mean of the differences between observations and hindcast relative to the mean observed SWH (e.g. van der Westhuysen et al. 2012). The scatter index is the RMSE relative to the observed mean (e.g. Musić and Nicković 2008). The latter, being dimensionless, is more appropriate to evaluate the relative closeness of the hindcast to the observations at the different locations compared with the RMSE which is representative of the size of a ‘typical’ error. The statistics in Table 2 are computed for all H_s and for $H_s \geq 90$ th percentile. Figure 4 compares a 5-month time-series of hindcast and measured SWH at Athos and Avgo buoy locations. Figure 5 also compares the hindcast SWH against in situ observations. In this case, the comparison is done through merged scatter and quantile-quantile plots as well as through log-normal plots and is shown for five locations: Athos, Lesvos, Mykonos, Avgo and Crotona wave buoys. The 45° reference line and a best-fit line passing through the origin are superimposed on the scatter plots. The wave roses in Fig. 6, presented for the same locations as in Fig. 5, show how well the directions of wave propagation are represented in the hindcast.

Table 2 reveals an overall reasonable agreement between measured and hindcast SWH. Nevertheless, the agreement varies for the different locations and depending on the percentile above which wave heights are considered. For all H_s , the correlation coefficient R ranges from 0.78 (Rhodes) to 0.93 (Athos). RMSE is from 0.29 m (Crotona) to 0.46 m (Santorini) and scatter index from 0.34 (Avgo) to 0.62 (Rhodes). The relative bias is from -0.14 (Rhodes) to 0.18 (Athos). In general, the statistics at Rhodes and Santorini are apparently worse than at the rest of the locations with scatter index > 0.5 and $R < 0.85$. For $H_s \geq 90$ th percentile of the observed SWHs, R has deteriorated with values as low as 0.3 (Santorini) and as high as 0.87 (Athos). RMSE is from 0.57 m (Crotona) to 0.93 m (Santorini) and scatter index from 0.23 (Mykonos) to 0.6 (Rhodes). Relative bias is from -0.34 (Rhodes) to 0.03 (Monopoli). A negative relative bias has been computed for all locations but Athos and Monopoli (relative bias = 0 at Mykonos) revealing that the model mostly overestimates observed SWHs at higher percentiles at the examined locations. As for all H_s , the performance of the model at Santorini and Rhodes is the worst, followed by this at Syros. Relatively poor statistics are obtained at these locations which

are the least exposed in the Aegean Sea. At the more exposed buoy locations examined in the Aegean and Ionian Seas (for simplicity, the Ionian Sea is considered in this study to occupy all the examined domain lying westwards of Crete) the model performance is rather fair.

Figure 4 shows a good agreement between hindcast and measured SWH at Athos. Medium to higher range SWHs are well reproduced by the model with a modest overestimation of the highest SWH peaks and an alternation between over and under estimation in the medium range. In the lower wave height range, moderate model underestimation takes place. At Avgo, an exacerbation of the model overestimation at high SWH values is observed, at occasions exceeding 1 m. However, lower SWHs are better reproduced at this location. It should be noted that Athos and Avgo are the only wave buoys available for this study that may approximate offshore wave conditions (normally > 50 km from shore) with distances from shore of about 30 km (< 10 km for the other buoys). Our model setup was designed to reproduce offshore conditions but may not be suitable for nearshore conditions where—as it will be described later on in this section—a higher resolution wind and wave model would be more appropriate, especially in the case of offshore blowing winds (Cavaleri and Sclavo 2006).

Figure 5 depicts the pattern of the agreement between hindcast and observed SWHs for different SWH value ranges (in the following, the discussion is for all ten locations examined although not all of them are shown in Fig. 5). All plots demonstrate that the model overestimates high SWH values at all locations. Depending on the location, the overestimation is less or more severe, is linked to a different quantile and is more or less consistent over the SWH range where is observed. For example, at Athos, waves above 2.4 m, representing 4.5 % of the observations (0.955 quantile), have a higher probability of occurrence in the hindcast than in the observations as it is apparent from the quantile-quantile plot (numbers and percentages mentioned are approximate). The plot shows that this probability difference increases with increasing wave height except from the few most extreme wave events in the time-series for which hindcast and observations come closer together. The maximum quantile difference is 0.78 m and has a probability of 0.3 % (0.997 quantile). The scatter plot illustrates that the model consistently overestimates $H_s > 3.6$ m whilst the scatter around the 45° line is greater for $H_s < 3.6$ m. In fact, both plots reveal that waves below 2 m are mostly underestimated by the model. In accordance, the log-normal plot (SWH is divided in bins of 0.5 m) shows that waves less than 2.5 m occur less frequently in the hindcast, waves above 4 m occur more frequently, whilst waves in between have frequencies of occurrences that are close together with no consistent pattern of superimposition. At Athos, Mykonos, Crotona and Monopoli, the SWH overestimation occurs at quantiles with probabilities less than

Fig. 5 Merged scatter quantile-quantile plots (*left column*) and log-normal plots (*right column*) comparing WAM hindcast SWH and in situ measurements at different wave buoys. Superimposed on the merged scatter quantile-quantile plots are the 45° reference line (*discontinuous line*) and a best-fit line passing through the origin (*solid line*)

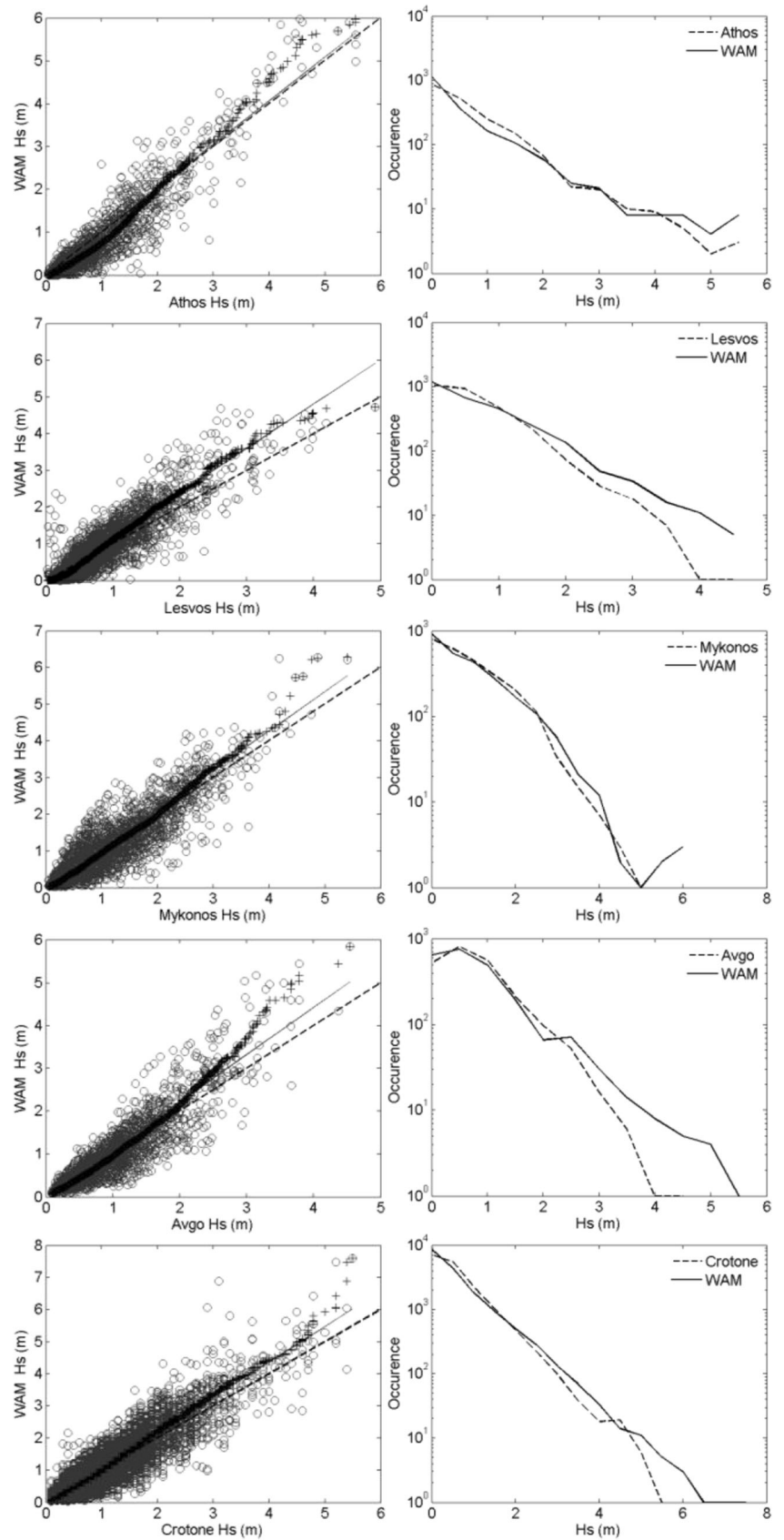
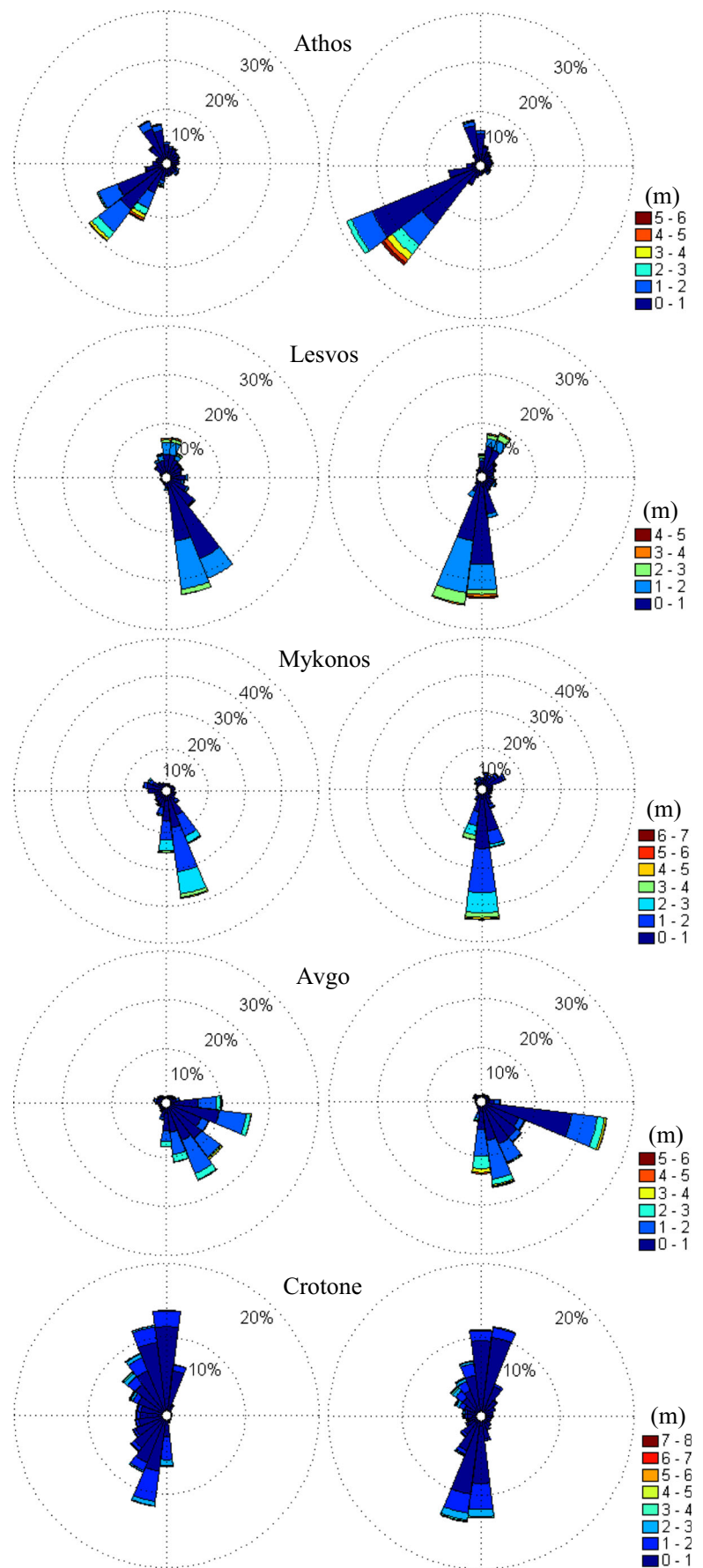


Fig. 6 Wave roses comparing WAM hindcast output (*right*) and in situ measurements (*left*) at different wave buoys. The direction to which the waves are travelling to is depicted



10 %. Avgo and Dia follow with the overestimation mostly occurring at quantiles with probabilities not greater than 17 %. At Lesvos as well as at Syros, Rhodes, and Santorini, the hindcast SWH overestimation is seen at quantiles with probabilities greater than 30 %. At Santorini as much as 50 % of the observed SWH values are overestimated in the model results. The largest SWH deviations at high quantiles are estimated for Rhodes and then for Avgo where hindcast SWHs may occasionally exceed measured SWHs by more than 1.5 m, as it is also apparent from the log-normal plot. Similarly to Athos, the model somewhat underestimates SWH at lower quantiles at most locations. Scatter plots show the greater scatter at Rhodes, Santorini and Monopoli. Moderate hindcast peaks that are not present in the measurements are seen at Lesvos and Monopoli.

Figure 6 shows that the main direction of wave propagation is generally well represented in the hindcast. Deviations that are noticeable occur at Lesvos, Syros, Rhodes and Mykonos. Thus, for Lesvos, the model simulates waves going mainly towards S-SW whilst the observations show that the main direction of propagation is towards SE. A similar shift from S-SE to S-SW directions is also the case for Syros and Mykonos. For Rhodes, the shift of the main wave direction is from NE-E in the observations to E-SE in the hindcast. Overall, a clockwise shift of the main wave direction is the case for many of the examined locations. Such directional shifts may be partly responsible for the statistical errors presented in Table 2, as it will be explained in the following paragraph.

The above comparisons demonstrate a reasonably good statistical agreement between the model output and the in situ observations at most locations when the entire SWH range is considered. This agreement is often better than that obtained by other high resolution wave hindcast studies for the Mediterranean Sea (Musić and Nicković 2008; Ratsimandresy et al 2008). Nevertheless, an overestimation of peaks is common. In general, it could be said that the agreement between the hindcast and the in situ measurements deteriorates at nearshore regions characterised by complex topography and where obstacles are present in the main fetch direction. For example, Rhodes buoy is surrounded by land

with a number of small islands present in the main fetch direction which is from SW-W. Similarly, Santorini receives waves that come mainly from N crossing numerous islands just north of it. At Lesvos (Fig. 6), the clockwise shift in the main direction of propagation from SE to S-SW means that waves cross a more complex topography with a smaller fetch to reach the buoy. The spatial resolution of the wave model is not adequate to resolve these fine bathymetric features. In addition, the spatial resolution of the wind model, which provided the forcing winds for the wave model, is incapable to reproduce the associated fine orographic effects, introducing errors to the wave hindcast. As stated by Cavaleri and Sclavo (2006), if the wind is blowing offshore, the wave data can be substantially wrong till at least 50 km from the coast. Such features may explain the less favourable agreement between hindcast and observed SWHs found at the aforementioned locations. On the other hand, waves meet less obstacles on their way to Crotona, Athos or Mykonos, which may explain the better agreement found in this case.

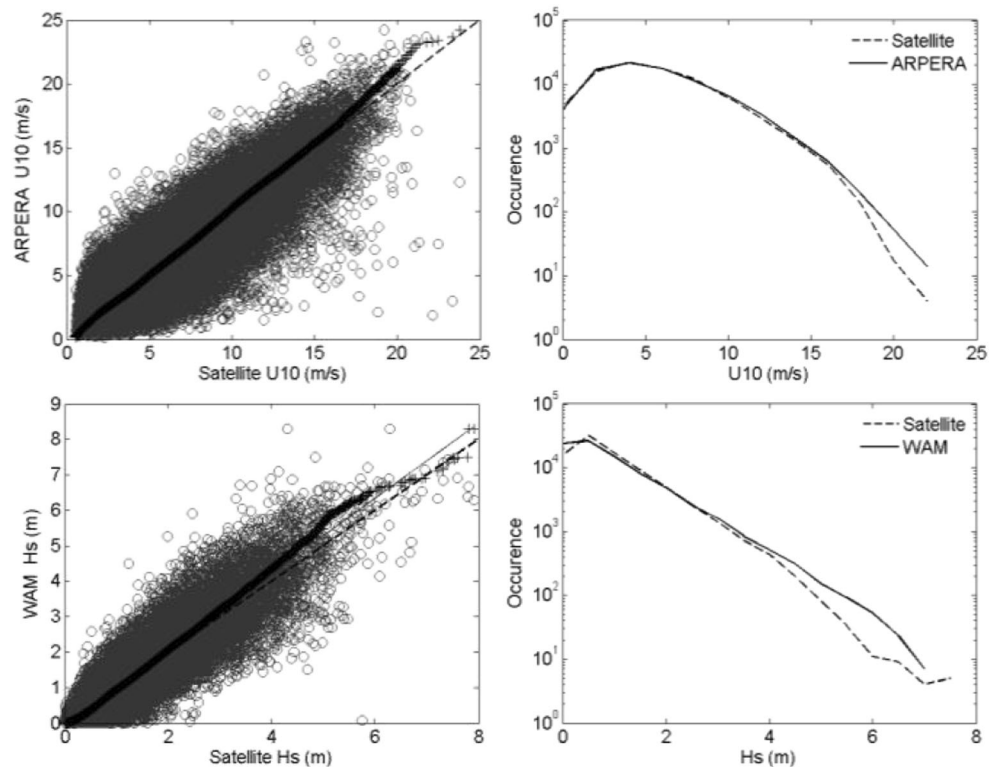
Table 3 shows the statistical parameters of the comparison between the model hindcast SWH and the satellite SWH data. Figure 7 compares both hindcast wind speed U_{10} and SWH with satellite U_{10} and SWH through merged scatter quantile-quantile plots and log-normal plots. Figure 8 depicts the spatial distribution of R , relative bias, and scatter index for all H_s values (top row) and for $H_s \geq 90$ th percentile (bottom row). The statistical parameters in Fig. 8 have been computed for each 0.5° grid cell individually on a sample that has been derived by accumulating the collocated model-satellite data per satellite pass over the successive satellite passes. For all H_s values, a sample size of 100 collocated model-satellite pairs was set as a minimum to compute the statistics. For $H_s \geq 90$ th percentile, the minimum sample size was set to 30 because of data availability constrains. It should be taken into consideration that this sample size may not be sufficiently large to guarantee the robustness of the computed statistics.

Table 3 shows that the model hindcast SWH compares well to the satellite SWH. R is 0.9 for all H_s and 0.7 for $H_s \geq 90$ th percentile. Respectively, RMSE is 0.38 and 0.71 m, scatter index is 0.34 and 0.24 whilst relative bias is 0.04 and 0. Figure 7, in agreement with Fig. 5, confirms some

Table 3 Statistical parameters of the comparison between the model hindcast SWH and satellite altimeter recordings

| | All H_s | $H_s \geq 90$ th percentile |
|---------------------------------------|-----------|-----------------------------|
| N | 83,867 | 8358 |
| R | 0.9 | 0.7 |
| $\bar{X}_{\text{obs}}(\text{m})$ | 1.12 | 2.93 |
| $\bar{X}_{\text{hindcast}}(\text{m})$ | 1.08 | 2.94 |
| Relative bias | 0.04 | 0 |
| RMSE (m) | 0.38 | 0.71 |
| Scatter index | 0.34 | 0.24 |

Fig. 7 Merged scatter quantile-quantile plots (*left*) and log-normal plots (*right*) comparing the corrected ARPERA hindcast wind speed (*top row*) and the WAM hindcast SWH (*bottom row*) to the respective satellite measurements



overestimation of satellite SWH by the model at high quantiles. It is seen that wave heights above 2.5 m, representing 7 % of the observations (0.93 quantile) have a higher probability of occurrence in the hindcast than in the observations. The probability difference increases with increasing wave height up to waves of about 6 m. The maximum quantile difference is 0.75 m and has a probability of occurrence of no more than 0.1 % (0.999 quantile). Occurrence probabilities converge for the most extreme values in the dataset. The scatter plot reveals that waves between 3.5 and 5.5 m are the most scattered and that the few highest satellite recordings are actually mostly underestimated by the model. The described patterns of agreement between hindcast and satellite SWH match well those observed for U_{10} .

Figure 8 reveals that the hindcast SWH is of good quality over most of the studied domain when all data values are taken into account. R is greater than 0.85 except for few grid cells. Exceptions are largely constrained in the Aegean Sea near the coast. Over Sporades islands and the eastern Cyclades islands R reaches its lowest range with values of 0.6–0.7. Relative bias is less than ± 0.1 in most of the domain. Positive biases, indicating higher altimeter than hindcast SWH, persist in the Ionian Sea and south of Crete with relative bias > 0.1 (< 0.2) present over the northern part of the former region and within the latter. Positive biases are also found in the northern Aegean Sea (< 0.2). Positive values of this statistic near the coast may be attributed to inaccuracies of the satellite

recordings as well as of the hindcast since, as stated by Queffeuilou and Bentamy (2007), some altimeter data can go through the quality test though still being affected by the land presence in the footprint, resulting in higher values of SWH. Negative biases prevail in the southern Aegean, reaching values as low as -0.25 over the Cyclades and the northern Dodecanese islands. Scatter index is clearly higher in the Aegean Sea compared with the rest of the domain. There, scatter index is generally between 0.4 and 0.6, reaching higher values near certain coastal locations. Over the southeastern exit of the Aegean Sea and outside this basin, scatter index is typically less than 0.4. Accordingly, RMSE (not shown) is mostly in the range of 0.4–0.7 m in the Aegean Sea and is less than 0.45 m otherwise. For $H_s \geq 90$ th percentile, R values are quite variable. They are generally greater than 0.6, often greater than 0.7. The few grid cells with $R < 0.6$ are scattered over the studied area. Relative bias is positive in the Ionian Sea (< 0.15) and negative in the Aegean Sea (≥ 0.4), particularly in the southern Aegean. In general, the overestimation of satellite SWH by the model in the central and southern Aegean Sea is in good agreement with the overestimation found at the wave buoys located within this region (all Greek buoys in Fig. 3 but Athos) for high waves. Scatter index for $H_s \geq 90$ th percentile also increases noticeably in the Aegean Sea, mostly in its southern part, as it was also the case for all H_s values. RMSE in this region can be up to 1.2 m; otherwise, it does not exceed 0.8–0.9 m. It is added that the equivalent comparisons

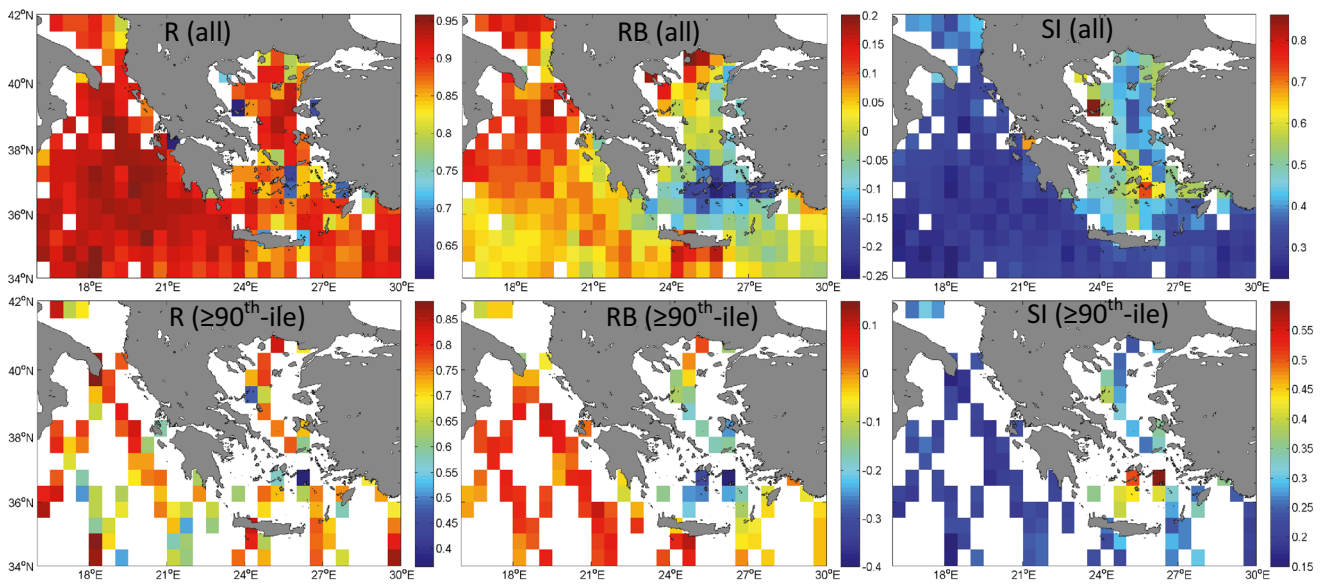


Fig. 8 Spatial distribution of the statistical parameters R , Relative Bias (RB) and Scatter Index (SI) (from left to right) of the comparison between WAM hindcast SWH and satellite SWH; for all H_s (top row) and for $H_s \geq 90^{\text{th}}$ percentile (bottom row)

between corrected model U_{10} and satellite U_{10} data (not shown) resulted in spatial distributions of R and relative bias that generally match the ones described above for H_s , confirming the strong relation of the wave fields to the forcing wind fields found in many studies (e.g. Cavaleri and Sclavo 2006).

On the whole, the validation of the hindcast against in situ observations and satellite data has shown that one could rely on the hindcast wave height and direction to assess the offshore wave climate of the Hellenic Seas everywhere but in the Aegean Sea, particularly its southern part. The highly sheltered nature of the Aegean Sea together with its highly complex topography, especially in the south, makes it a region where genuine offshore wave conditions are limited and as a result, nearshore very high resolution wind and wave modelling could be more appropriate. It was shown, through the validation, that it is mainly the extreme wave conditions that are expected to be less reliable in the Aegean Sea, since those are often substantially overestimated in the hindcast. This would result in extreme wave climate statistics that are on the conservative side, i.e. having values greater than those expected in reality. Although this situation is more desirable than the opposite in engineering applications, such as, for example, the design of marine structures, a rough idea of the bias should exist to avoid unnecessary structural costs.

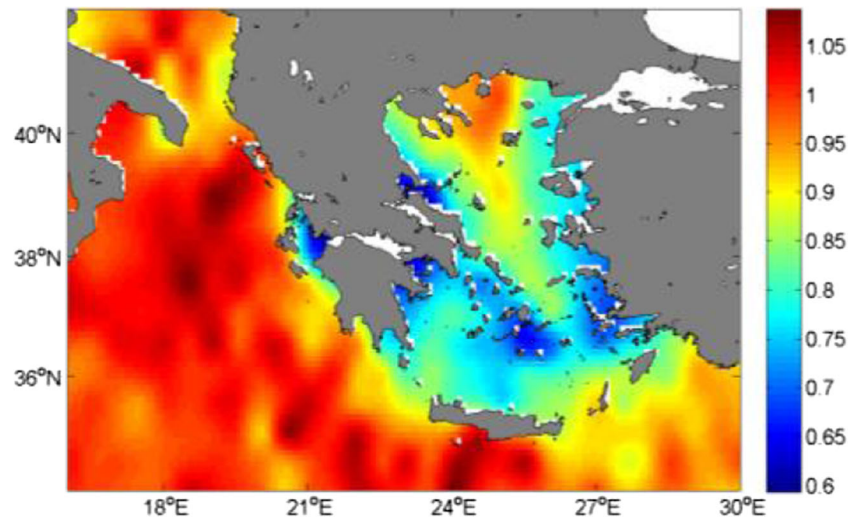
3.2 Calibration

To improve the original model SWH values, with a focus on the extreme wave height range, simple linear regression analysis was employed. The adjusted model dataset was then used in the computations of the extreme wave climate statistics

presented in the following sections (Sects. 4, 5 and 6). Extreme wave climate statistics were also computed using the original model hindcast hence obtaining an insight on the implication of the model bias on the results (reference to this implication is limited to the conclusions in Sect. 7). The applied SWH adjustments are briefly described below. It is highlighted that it is out of the scope of this paper to provide a comprehensive calibration of the original wave hindcast as well as a thorough validation of the adjusted dataset. This can be a complex task and as such it is often the primary objective of research articles (e.g. Caires and Sterl 2005; Cavaleri and Sclavo 2006). Instead, a simple ad-hoc empirical method is used that serves the main objectives of the present study.

A best-fit linear model of the form $y=ax$ (satellite data= $a \times$ model data) was fitted to the samples of the collocated model-satellite SWH pairs per cell (same as for Fig. 8), and the derived slopes a were then interpolated to the wave model grid to obtain the coefficients for adjusting the original SWH hindcast according to the relationship adjusted hindcast= $a \times$ original hindcast. In general, this zero intercept linear fit was found to better represent the upper most wave height range than a nonzero intercept fit which often led to a non-trivial undesirable underestimation of the probabilities of occurrence of extreme events in the adjusted hindcast. On the other hand, the use of the specific fit often resulted in a bias between adjusted hindcast and observations that was higher than the one obtained with the original hindcast when the entire SWH range was considered. In general, an exploration of the regression analysis results indicated that the adjusted SWH hindcast is more appropriate than the original SWH hindcast to obtain extreme wave climate statistics but is less suitable to compute the mean wave climate, for which the original dataset was

Fig. 9 Spatial distribution of the adjustment coefficients, a (adjusted SWH hindcast = $a \times$ original SWH hindcast)



used. In the following, the interpolated adjustment coefficients, a , are shown in Fig. 9. Figure 10 shows how the adjusted SWH hindcast compares with the independent in situ wave measurements whilst Fig. 11 shows the distribution of relative bias and scatter index for $H_s \geq 90$ th percentile after the adjusted SWH hindcast is compared back to the satellite SWH recordings used for the adjustments.

Figure 9 shows that the coefficient a is in the range of 0.9–1.1 outside the Aegean Sea with most values being close to 1. Some patchiness is evident in the distribution, also in areas where uninterrupted wave propagation would suggest a rather smooth distribution. This may be associated to the randomness implicit in the calibration procedure (Cavaleri and Sclavo 2006). For instance, the data used for best-fit at neighbouring cells could be potentially associated to different events and at the same time the model responds differently to different situations. Also, the accuracy of the interpolated model output to the different satellite tracks varies. In addition, there may be a difference in the accuracy with which the different satellite altimeters measure SWH. For example, Cavaleri and Sclavo (2006), in a similar model data calibration exercise, found that the best-fit slopes for ERS data were on average 3 % larger than those related to TOPEX data. Nevertheless, the tight

range of the coefficient variation should not have severe implications on the computed climate statistics. In the Aegean Sea, $a > 0.9$ is obtained over the northern part of the basin and away from the coastline to the east and west. The adjustment coefficient decreases towards the central and southern Aegean, taking its lowest values (0.6–0.8) over the Cyclades islands, the northern Dodecanese islands and north of Crete. Values near the coast, where empty cells appear in Fig. 8 as a result of insufficient collocated model-satellite data pairs, should be considered the least reliable as these were obtained through extrapolation.

Figure 10, in comparison with Fig. 5, reveals that the adjusted SWH hindcast represents much better the in situ measurements of extreme SWH (the discussion here is also for those buoys not shown in Figs. 10 and 5). In particular, the probabilities of occurrence of extreme events—which are more important in the calculation of long-term climate statistics compared with serial correlation—are now much closer to the 45° reference line at most buoy locations. The improvement is particularly evident at Avgo and Santorini, where the discrepancies between hindcast and observations before the adjustment were from the largest. Significant improvement is also seen at Lesvos, Syros and Dia whilst this is small at

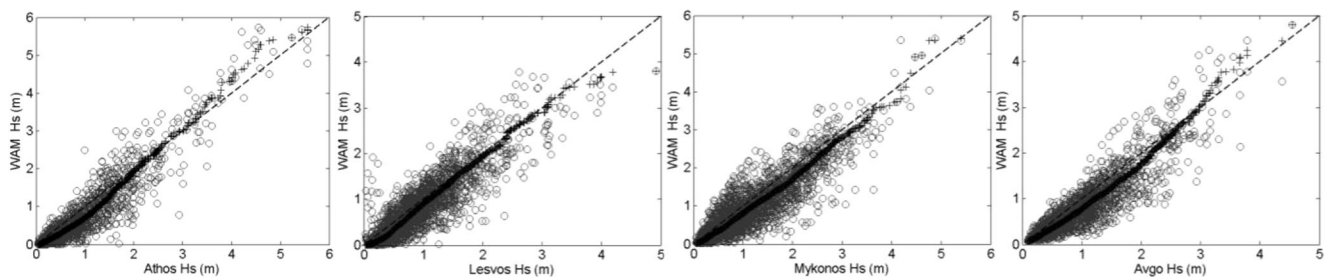


Fig. 10 Merged scatter quantile-quantile plots comparing adjusted WAM hindcast SWH and in situ measurements at different wave buoys. Superimposed is the 45° reference line

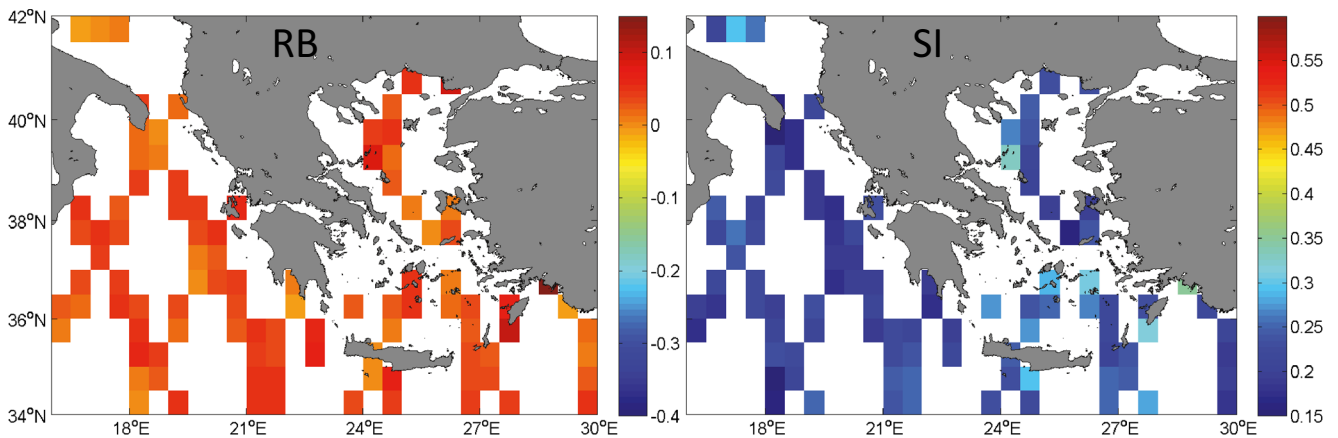


Fig. 11 Spatial distribution of the *Relative Bias* (left) and *Scatter Index* (right) of the comparison between adjusted WAM hindcast SWH and satellite SWH for $H_s \geq 90$ th percentile

Athos, Mykonos and Crotona where the original hindcast was already of good quality. At Rhodes, although the adjusted hindcast performs better, non-trivial overestimation at high quantiles remains. However, this is an especially sheltered buoy where the adjustment coefficient has been obtained through extrapolation and, as mentioned earlier, output at such locations is expected to be the least reliable.

Figure 11, in comparison with Fig. 8, shows that both relative bias and scatter index for $H_s \geq 90$ th percentile improve after the hindcast adjustment, particularly in the southern half of the Aegean Sea where the most problematic values were obtained before adjustment. Specifically, relative bias is now in the range -0.005 to 0.1 compared with -0.42 to 0.1 originally. Positive values are now obtained over nearly the entire domain. Despite an occasional increase in the absolute relative bias towards positive values in Fig. 11 (e.g. north Aegean), maps of the 99th percentile of H_s and of maximum H_s derived separately for the collocated satellite observations, the original hindcast and the adjusted hindcast (not shown) show an improved agreement of the adjusted hindcast to the satellite observations with some overestimation remaining in the hindcast. Scatter index is everywhere better after hindcast adjustment with its range becoming 0.15 – 0.35 compared with 0.15 – 0.6 originally. RMSE is now 0.35 – 0.85 m compared with 0.4 – 1.2 m originally.

The aforementioned results give us the confidence that the extreme wave height climate statistics computed with the use of the adjusted model SWH hindcast and presented below are of reasonable quality.

4 Hindcast wave climate

Figure 12 shows the spatial distribution of the mean, standard deviation and maximum SWH for the period 1960–2001. It is seen that the mean SWH is greatest west and east of Crete (see Fig. 2 for geographical locations), reaching 1.37 m in both regions. In the Aegean Sea, far from the mainland and up to the line connecting the islands of Skyros and Limnos, values of 1–1.2 m are typical. North of this line, mean SWH is markedly reduced. In the Ionian Sea, a gradual reduction can be seen from south to north from more than 1.2 m to less than 1 m at the entrance of Otranto Strait. The described spatial pattern is comparable with that reported by Soukissian et al. (2008) on the winter mean. Nevertheless, in agreement with Queffeuilou and Bentamy (2007), higher winter mean values have been observed in this study (not shown), occasionally exceeding 2 m. A pattern similar to that of the mean is found for the standard deviation of SWH with the main differences located southeast of Crete and north of the Cyclades complex.

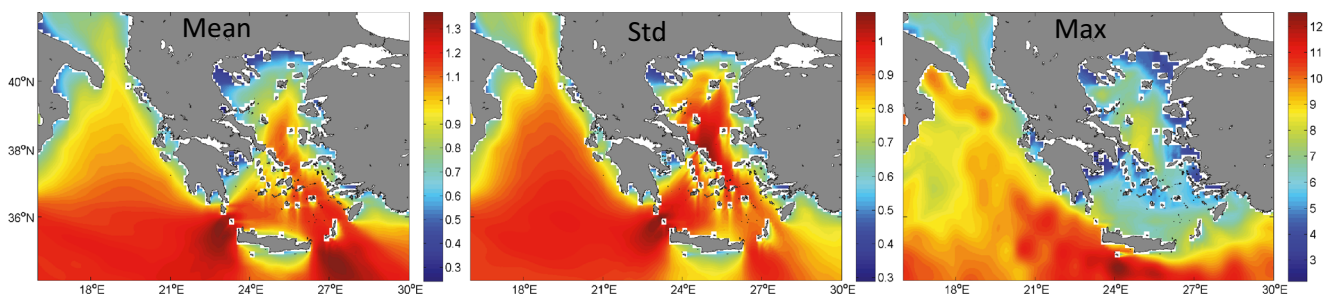


Fig. 12 1960–2001 mean SWH (left), standard deviation of SWH (middle) and maximum SWH (right) in meters

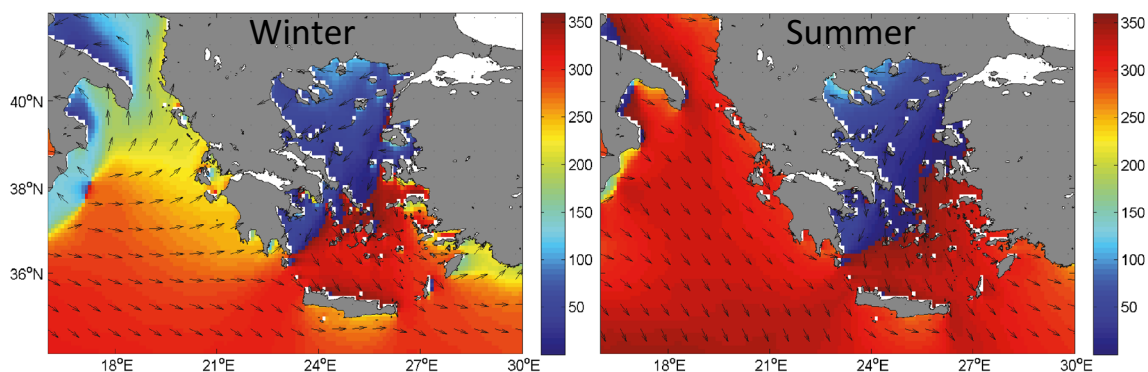


Fig. 13 1960–2001 mean wave direction in degrees for winter (*left*) and summer (*right*). Colour scale indicates the direction from which the waves are coming from (0° wave direction is from North)

In the former case, the SWH variability is reduced relative to the mean whilst it is increased in the latter. The distribution of the maximum SWH deviates from that of the mean. In this case, waves as high as 11–12 m embrace the west coasts of Crete and Gavdos islands and follow an arc that lays close to the southern boundary of the domain and fades towards the east. In the Aegean Sea, the highest SWH values are seen north of the Cyclades complex, especially along the east coasts of Andros and Tinos islands and are between 7 and 8.5 m. A peak is also seen off the coasts of Thessaly. In the Ionian Sea, the maximum SWH gradually decreases to the northwest reaching 8 m offshore the Italian coastline. It increases again towards the Salento peninsula.

The pattern of the mean wave direction (not shown) is very similar to the winter mean shown in Fig. 13 (*left*) with the directions of propagation outside the Aegean Sea and around its southeastern boundary being more aligned to the north. This northerly shift is typically less than 25° . Thus, as seen in Fig. 13, the waves in the Aegean Sea follow an arc starting at the Dardanelles straits at north, where they are northeasterly, turning around the Cyclades islands to northwesterly and passing through the straits between Crete and Rhodes islands to travel eastwards into the Levantine basin. In the Ionian Sea, westerly waves are dominant being more northwesterly in the southern part of the domain and more southwesterly in the northern part. In summer (Fig. 13, *right*),

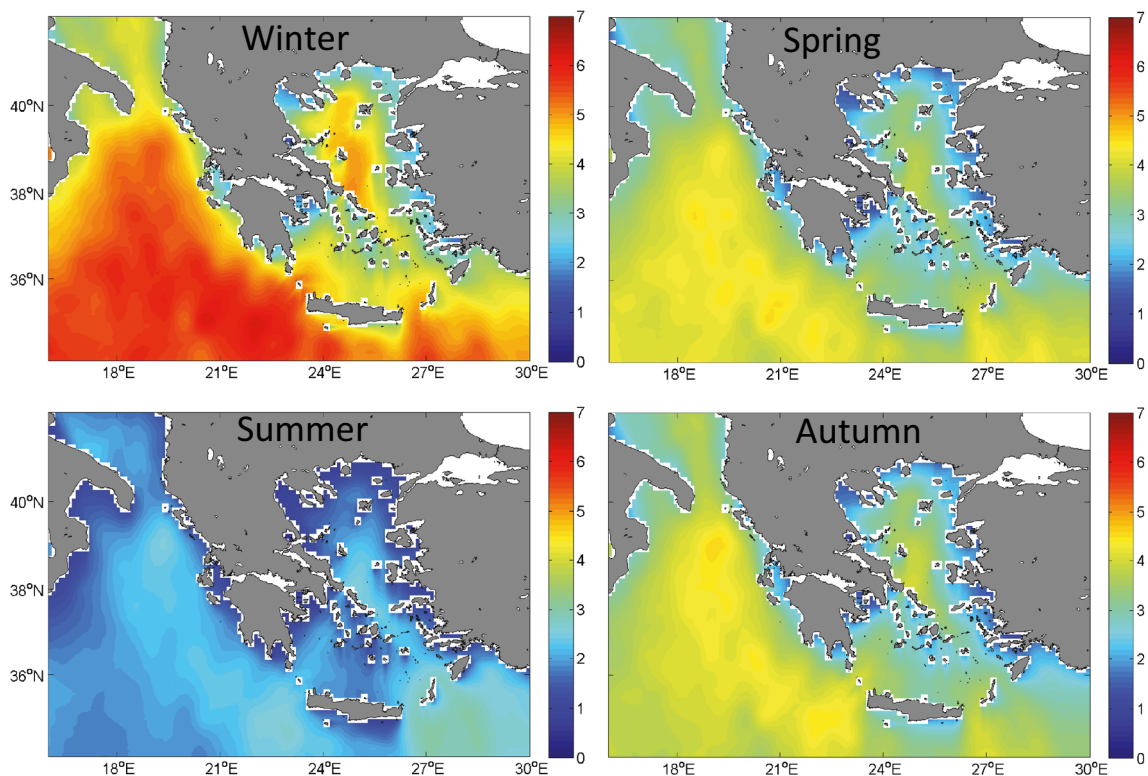


Fig. 14 1960–2001 99th-tile of SWH in m for winter (*top left*), spring (*top right*), summer (*bottom left*) and autumn (*bottom right*)

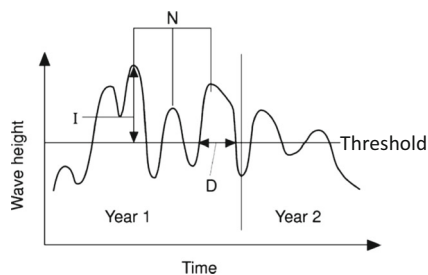


Fig. 15 Definition of parameters that characterize extreme wave event statistics. Here, *Threshold* is the 99th-ile of total SWH, *N* the annual number of extreme events, *D* their duration and *I* the intensity of these events (modified from Weisse and Günther 2007)

northerly waves are dominant over the entire domain, coming from the northwest in the Ionian Sea and following the aforementioned arc in the Aegean Sea which is now more aligned with the north-south axis. Spring wave direction resembles that of winter and autumn wave direction resembles that of summer everywhere apart from the Ionian Sea above $\sim 36^\circ$ N. There, a relatively sharp gradient from northerly to southeasterly directions is observed in both seasons bringing autumn mean wave directions close to those of winter in the region whilst making spring mean wave directions being the most southeasterly in comparison. Soukissian et al. (2008) refer to the same arc of propagation in the Aegean Sea described herein for both wind and wave propagation, which are generally found to be in good agreement. Lionello and Sanna (2005)

also report similar seasonal mean wave directions. Winter wave propagation is attributed mainly to the influence of the northerly Bora winds in the Aegean Sea and a combination of the northwesterly Mistral and southerly Sirocco in the Ionian. The influence of the Sirocco wind increases in spring and autumn. In summer, wave propagation is dominated by the northerly Etesian winds in the Aegean and by Mistral in the Ionian Sea (e.g. Chronis et al. 2011; Lionello et al. 2006)

To examine the extreme wave climate of the Hellenic Seas, the 99th percentile of SWH (hereafter 99th-ile) - a measure that is routinely adopted to study extreme sea states (e.g. Weisse and Günther 2007; Appendini et al. 2014) - is employed in this study. Figure 14 shows the spatial distribution of this parameter for each season. The winter distribution (top left) is representative of that of the long-term 1960–2001 99th-ile (Fig. 16, top left). The highest values are observed in the southeastern Ionian Sea and are about 6 m. In general, values greater than 4.5–5 m prevail in the Ionian Sea and over the southern boundary of the examined domain. In the Aegean Sea, high values of 4.5–5 m are seen along the east coasts of Euboea, Andros and Tinos islands and to the NE. Similar values are observed over the Crete-Kythira and Crete-Karpathos straights. Otherwise, values are about 4 m except within the Cyclades complex and near the mainland coast where relatively low values prevail. In summer (bottom left), the maximum 99th-ile appears around the Crete-Rhodes straights and in the Levantine Sea reaching values of more

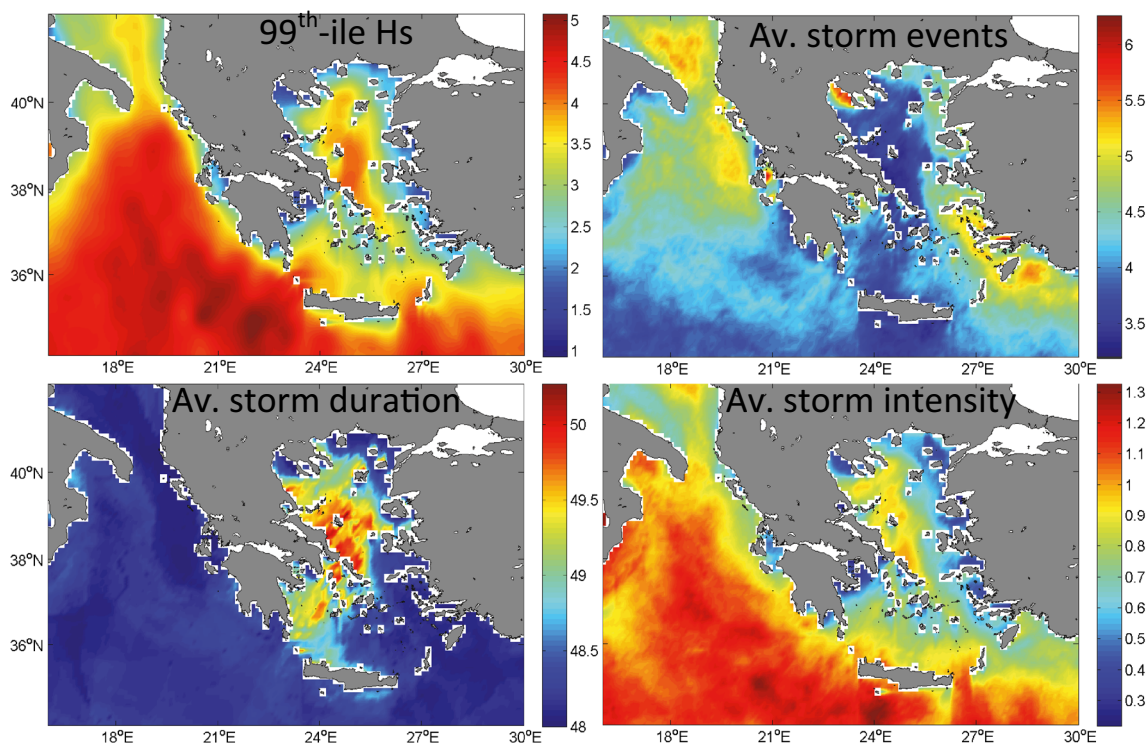


Fig. 16 1960–2001 99th-ile of SWH in m (top left), the average annual number of events exceeding the 99th-ile (top right), their average duration in hours (bottom left) and their average intensity in m (bottom right)

than 3 m. This is in agreement with the observations of Queffelec and Bentamy (2007) on mean summer SWH. Otherwise, similarly to winter, high values of 2.2–2.6 m are observed along the east approaches of the Cyclades islands. However, in this case, they occupy a smaller area to the N-NE. Also, in agreement with the winter distribution, values reach 2.7 m in the southeastern Ionian Sea. Generally, in the Ionian Sea, the 99th-ile reduces gradually westwards as the distance from west Greece increases. Spring (top right) and autumn (bottom right) present distributions similar to that of winter with a relative intensification of the severe wave climate in the eastern part of the domain in spring, similarly to summer, and a relative weakening of the sea states in the western part of the domain in autumn. Comparable values of up to 4.6 m are observed in both seasons.

To study the storm characteristics of the area, we follow the methodology used in Weisse and Günther (2007). Specifically, the local long-term 1960–2001 99th-ile of total SWH is used as a threshold to determine severe wave conditions. As in Weisse and Günther (2007), exceedance statistics such as the annual number of extreme events, their duration and intensity are defined based on this threshold. Figure 15 shows the definition of these statistics schematically.

Figure 16 shows the value of the local 1960–2001 99th-ile of total SWH over the Hellenic Seas (top left), the average annual number of extreme events (top right), their average duration (bottom left) and their average intensity (bottom right). It is noted that each extreme value is selected so that it represents an independent event. This is interpreted as requiring a spacing of at least 72 h between events (Debernard and Røed 2008).

As mentioned above, the 1960–2001 99th-ile of SWH has a distribution that is very similar to the winter 99th-ile shown in Fig. 14 and described in a previous paragraph. Its range is between 1.6 and 5.1 m. Figure 16, top right, shows that the annual number of peaks over the 99th-ile threshold is higher in the north Ionian Sea and the western Aegean Sea close to the Turkish coastline, especially south of the Ikaria Trough. There, the set threshold is exceeded on average 4.5 to 5.5 times per year. In the southern Ionian, the southern Aegean Sea and southeast of Crete a typical range is 4–4.5 events per year. Otherwise, exceedance occurrences are between 3.2 and 4 events per year. Notably, along the eastern coasts of the Cyclades and Euboea islands the number of independent storms is one of the lowest despite the high threshold values observed. Few extreme events in a region of high thresholds

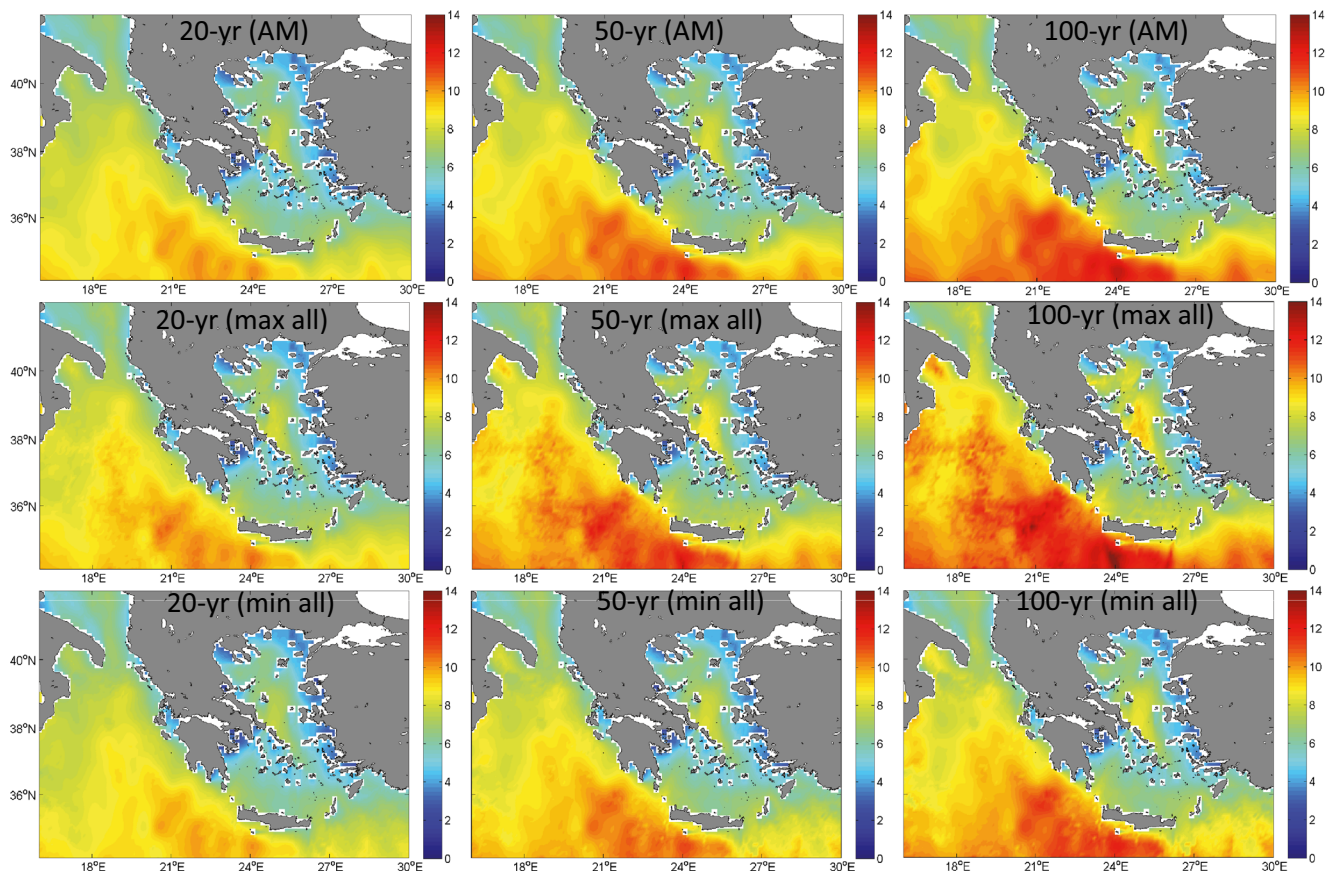


Fig. 17 SWH in meters for 20, 50 and 100 years return periods (left to right column, respectively) as derived with the AM method (top row), its maximum value (middle row) and its minimum value (bottom row) as

derived from all methods (AM and POT using different parameter estimation methods, e.g. ML, PWM)

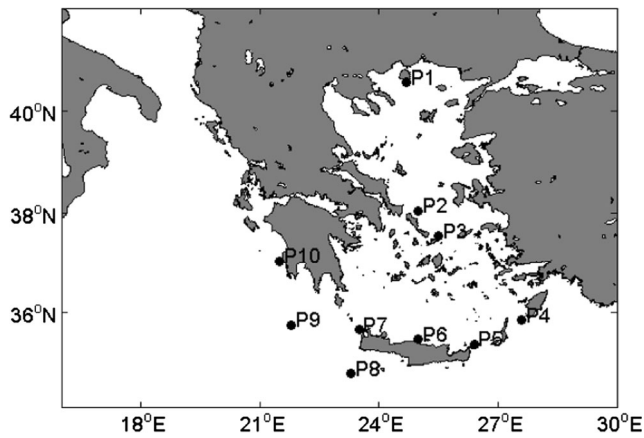


Fig. 18 Map of the locations where return level plots were extracted

should imply a longer duration of these events and vice versa. Figure 16, bottom left, shows that this is indeed the case in such regions in the Aegean Sea. There, the greatest average storm durations, exceeding 50 hrs, are observed. In general, the variability of the average storm duration is small with the values of this parameter being within the narrow range of 48–50.3 hrs. Figure 16, bottom right, shows that the average intensity of the severe wave events has a distribution that is rather patchy in appearance but is close to the one of the 99th-ile. In contrast to the latter, the biggest concentration of maxima now appears directly south of western Crete, with the maximum value of 1.33 m located south of the island of Gavdos. Also, relative high storm intensities of more than 1 m are now observed along the Italian coastline whilst storm intensity in the Aegean Sea seems to reduce faster than the 99th-ile eastwards.

5 Return periods

To estimate SWH return periods two well-known methods were used in this study, the annual maximum (AM) and the peaks over threshold (POT) methods. The generalised extreme value distribution (GEV) was used to fit the samples

of extremes generated by the AM method whilst the generalised Pareto distribution (GPD) was used to fit the samples generated by the POT. These distributions were fit to the samples using different parameter estimation methods namely the maximum likelihood (ml), the probability weighted moments (pwm) and the maximum product of spacing (mps) methods (mps is used only with GPD fitting). In the POT method, a threshold for each grid point was selected automatically based on two statistical measures: the *mean residual life plot* which is the plot of the mean exceedance over a threshold as a function of this threshold and the *dispersion index*, which is the ratio between the variance and the expectation of the number of peaks. For details on the extreme value analysis statistics employed in this study, the reader is referred to Coles (2001) as this is out of the scope of this study. Also, a comparative study of the AM and POT methods for the Dutch coastline is given by Caires (2009).

Figure 17 (top row) shows the 20-, 50- and 100-year return periods of SWH as obtained with the AM method. The middle and bottom rows show the maximum and minimum values of the respective return periods as extracted from all methods. The results obtained with the AM method have been chosen for display because of their smoother spatial variation compared with that of the POT method (non-trivial patchiness shown in Fig. 17 middle and bottom rows is mainly due to the POT-pwm method). Nevertheless, all methods resulted in a very similar spatial distribution and comparable magnitudes of the examined variable.

As seen in Fig. 17, the 20-year return period SWH acquires its maximum values over a broad region in the southeastern Ionian Sea and south of western Crete. Values reach up to 10.1 and 10.6 m when the minimum and the maximum of all methods is considered respectively. With increasing return period the return level SWH pattern resembles more the 1960–2001 maximum SWH pattern shown in Fig 12, with the highest values located south of west Crete. For a 50-year return period, maximum values reach up to 11.2 and 12.8 m when the minimum and maximum of all methods is considered respectively. For a 100-year return period, the above maxima become 12 and 14.8 m. In accordance with results

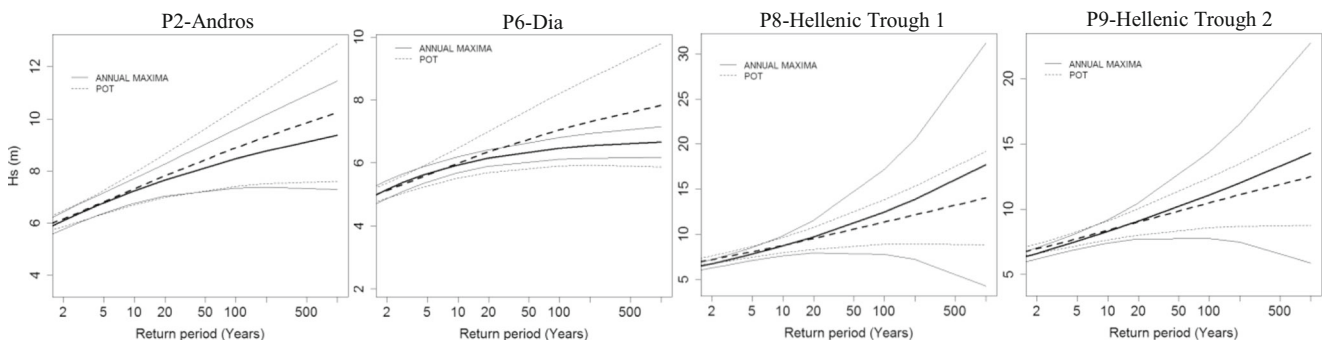


Fig. 19 Return level plots with confidence intervals (locations shown in Fig. 18)

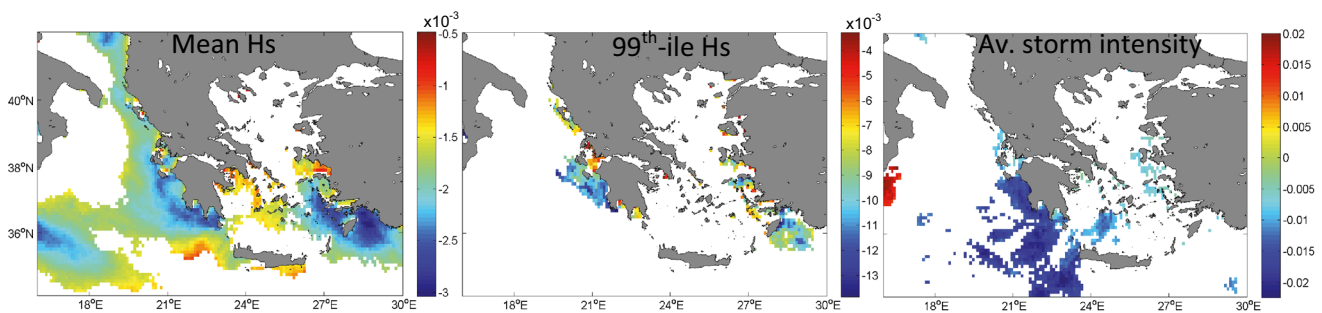


Fig. 20 Annual mean SWH (*left*), 99th-ile SWH (*middle*) and average intensity of extreme events (*right*) trend slopes in meters per year for statistically significant trends (5 % significance level)

in the previous section, high return values are found within most of the southern Ionian Sea and in the Levantine Sea south of Rhodes and Karpathos islands. They are similar in both cases and are mostly between 8.6 and 11 m for a 100-year return period, accounting for all methods. In the Aegean Sea, the highest SWH return levels are observed along the north-northeastern coasts of the Cyclades complex and the island of Euboea and reach up to 9.7 m for a 100-year return period. For the same return period, return levels in the north and southern Aegean Sea are mostly between 5 and 8 m whilst in the northern Ionian Sea are mostly between 7 and 10 m.

Figure 18 shows several locations for which return level plots were obtained. Figure 19 shows the return level plots at five of these locations. Return levels are drawn for return periods up to 1000 years and represent the AM-ml and POT-ml methods including estimates of confidence intervals. As expected, the difference of the results obtained with the two methods grows with the return period. So do the confidence intervals. For return periods up to 100 years, differences are below 0.6 m except for location P8 where the difference becomes 1.1 m. For return periods up to 1000 years, the aforementioned differences have a 1- to 2-fold increase at points P1–P6 in the Aegean Sea and P10 in the Ionian Sea whilst they have a 3- to 4-fold increase at points P7–P9 where the largest SWH return levels are observed. The maximum discrepancy for a 1000-year return period is obtained at P8 and is as high as 3.7 m. To conclude, for the Hellenic Seas, the choice of the method for estimating SWH return levels is not

that critical for return periods up to 100 years but may become so for higher return periods. Nevertheless, an important finding is that all methods, including the different parameter estimation methods, fall within the confidence intervals of the AM-ml and POT-ml methods which in all cases overlap producing no statistically significant differences.

6 Wave climate trend and variability

Wave climate trends were obtained based on the Sen's slope estimator, a non-parametric method for robust linear regression. The regression analysis was performed on the 42 yearly (1960–2001) and seasonal values of the mean and the 99th-ile SWH at each grid point. Subtrends within the 42-year period were also investigated. The calculated slopes were tested for statistical significance using the non-parametric Mann-Kendall test. Only those found significant at the 5 % significance level are presented in this section. In the following, a statistically significant trend is implied whenever reference to a trend is made unless stated otherwise.

Figure 20 shows trend slopes for the mean SWH, the 99th-ile SWH and the average intensity of extreme events. No increasing trends (i.e. positive slopes) are observed in the Hellenic Seas for any of these three parameters. As far as the mean SWH is concerned, a widespread reduction is present. In the Ionian Sea, this occupies the entire west Greek and Balkan continental shelf. It faints towards the west and towards the

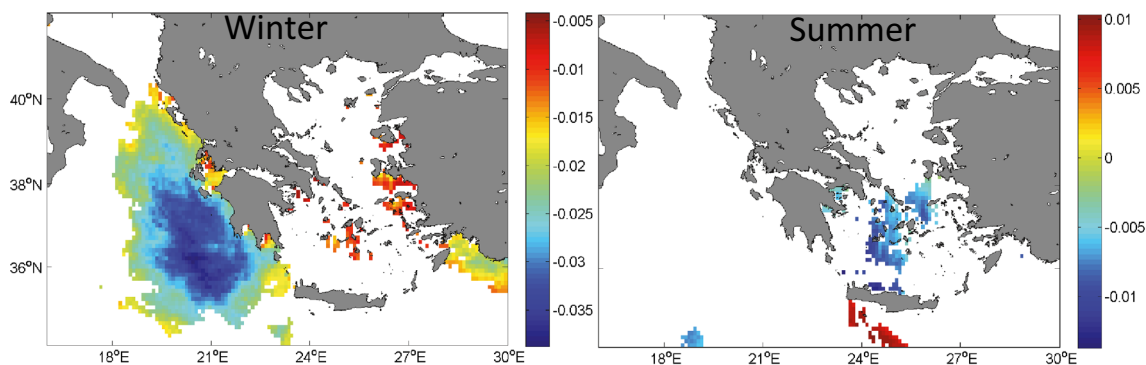
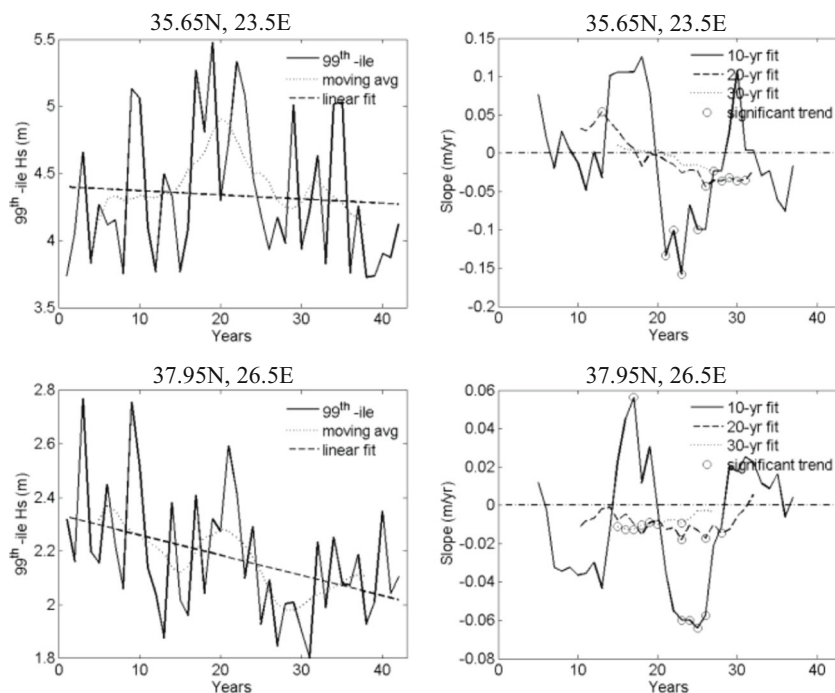


Fig. 21 Winter (*left*) and summer (*right*) 99th-ile SWH trend slopes in meters per year for statistically significant trends (5 % significance level)

Fig. 22 *Left column:* 99th-ile SWH interannual variability; superimposed is the moving average and the regression line. *Right column:* trend slopes resulting from 10-, 20- and 30-year moving linear fits. *Open circles* denote a significant trend



south but remains in most of the southwestern part of the examined domain. Negative slopes are also seen in the Aegean Sea over the southern Cyclades complex and eastwards from a curve connecting the islands of Chios, Ikaria and Karpathos. The same situation repeats south of eastern Crete. Slopes are small, as low as -0.3 cm/year (12.6 cm in 42 years). A relatively limited reduction is observed for the 99th-ile SWH. In this case, the reduction is focused west of Peloponnesus and off the northwestern Greece and at certain nodes eastwards from a curve connecting the islands of Chios, Ikaria and Rhodes, mainly south-southeast of Rhodes. Slopes are as low as -1.4 cm/year (58.8 cm in 42 years). In agreement, the average intensity of extreme events is also reduced with slopes as low as -2.5 cm/year (1.05 m in 42 years). This reduction occupies a broad region west-southwest of Peloponnesus and Crete. It is also seen in a zone running southwest from the islands of Milos and Folegandros (next to Milos to the east) and at a number of locations in the

Cyclades complex and the eastern-central Aegean Sea. This parameter as well as the 99th-ile increase over a substantial part of the Aegean Sea. However, this increase is statistically insignificant. The average annual number of severe events and their average duration showed no significant trends.

Seasonally, negative trends are present in both winter and summer and for both the mean and the 99th-ile SWH. Spring and autumn trends are mostly insignificant. The reduction of mean SWH in winter and summer (not shown) is small with slopes as low as -0.8 cm/year and -0.6 cm/year, respectively. However, these negative slopes are greater in comparison with those found for the annual mean SWH which could be explained by non-significant positive slopes dominant in autumn. The winter and summer 99th-ile trend slopes are shown in Fig. 21. In winter, negative trends as low as -4 cm/year (1.68 m in 42 years) are seen from the west Greek continental coastline to $\sim 18^\circ$ E. In the Aegean Sea, the pattern is similar to the one of the annual 99th-ile (Fig. 20) with some extra

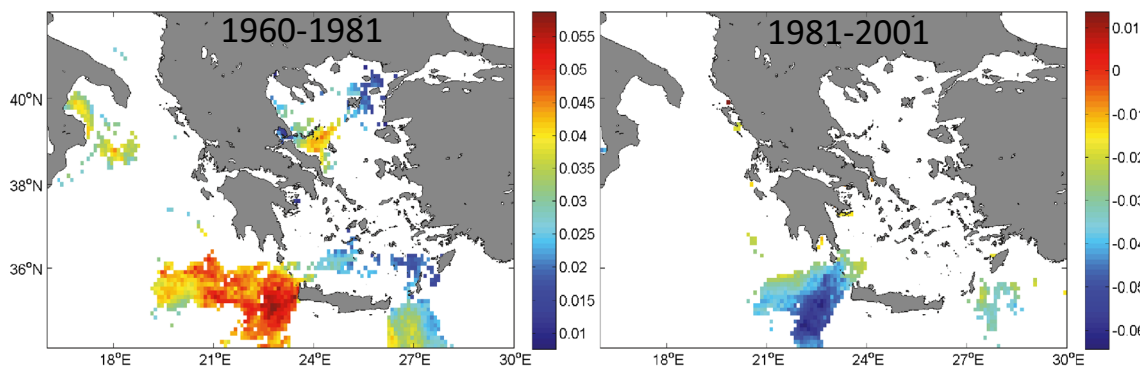


Fig. 23 1960–1981 (*left*) and 1981–2001 (*right*) 99th-ile SWH trend slopes in meters per year for statistically significant trends (5 % significance level)

locations of negative trends appearing in the Cyclades complex. Slopes are smaller than in the Ionian Sea. In summer, 99th-ile reduction is observed only in the Aegean Sea around the Cyclades islands with negative slopes as low as -1.5 cm/year (63 cm in 42 years). Positive slopes of up to 0.96 cm/year are seen south of Crete. Non-significant widespread increase of the 99th-ile is found mainly in autumn but also in spring.

The above results are generally in agreement with the results of previous studies. Specifically, Martucci et al. (2010) found a negative slope (-0.12 cm/year) for the mean annual SWH in the Ionian Sea in the period 1958–1999, at a location offshore the Italian coastline. In their study, in contrast to this work, this trend was found to be statistically significant. Lionello and Sanna (2005) found that the Mediterranean average annual SWH exhibits a statistically significant negative trend (-0.08 cm/year) in the period 1958–2001. They report that seasonally the negative trend is statistically significant only in winter (-0.2 cm/year) and is mainly due to a weakening of the action of the Mistral-Etesian pattern on waves during winter. In the present study, significant negative trends are also found in summer. This could be due to negative trends in the frequency and speed of the Etesian winds found in summer by Poupkou et al. (2011). The pattern of negative and positive slopes reported by Musić and Nicković (2008) for the 50th-ile and 90th-ile SWH at specific locations in the Eastern Mediterranean is also in agreement with the one found here for the mean and 99th-ile SWH.

Figure 22, left, reveals the interannual variability of the 99th-ile SWH at two locations: northwest of Crete island at 35.65° N, 23.5° E and south of Ikaria Island at 37.95° N, 26.5° E. Figure 22, right, shows the trend slopes resulting from 10-, 20- and 30-year moving linear fits. Open circles denote a significant trend. These plots help us to identify statistically significant subtrends present within the 42-year period. For example, the Mann-Kendall test gave no trend northwest of Crete for the 42-year period. Nevertheless, Fig. 22, top left, shows an increasing tendency in the 99th-ile in the first 19–22 years followed by a decreasing one in the remaining 20–23 years. Also, the 20-year linear fits in Fig. 22, top right, show a statistically significant increase (centred at year 13) between the 4th and the 23rd years of the 42-year time period examined. Statistically significant decreases are observed when the first few years of the time period are not taken into account. Similarly, south of Ikaria island the Mann-Kendall test revealed a decreasing trend for the 42-year period. However, the 10-year moving linear fits in Fig. 22, bottom right, reveal that the increasing tendency seen in Fig. 22, bottom left, between years 13 and 21 is statistically significant. Overall, a turning point in the tendency of the 99th-ile SWH within the 42-year period was identified between year 19 and 22 depending on location. Most locations were compliant with year 22 which corresponds to the calendar year 1981. Thus, the data set was divided in two parts, one representing the time

period 1960–1981 and the other representing the period 1981–2001. Trend slopes were then obtained for each of these two periods at each individual grid point. The results are presented in Fig. 23.

Indeed, Fig. 23 shows positive trends of the 99th-ile for the period 1960–1981 whilst negative trends pertain to the period 1981–2001. For the period 1960–1981, an increasing 99th-ile is observed west-southwest of the Crete-Kythira straights and south-southeast of the Crete-Karpathos straights where the most severe wave climate was found in the previous sections. Similar trends are also found off the island of Euboea. A smaller increase can be seen in limited areas in the northern and southern Aegean Sea. For the period 1981–2001, a decrease of the 99th-ile is constrained west-southwest of the Crete-Kythira straights and in a small area southeast of the island of Karpathos. In general, irrespectively of statistical significance, the period 1960–1981 is dominated by positive trends as high as 6 cm/year whilst the period 1981–2001 is dominated by negative trends as low as 6.4 cm/year. Opposing tendencies were also found when the mean SWH was examined in the two periods (not shown). Nevertheless, a statistically insignificant reduction of the mean SWH was common in both periods in most of the Aegean Sea including the northern, the central and most of the Cyclades region.

7 Conclusions

In this paper, the WAM wave model implemented over the Mediterranean Sea with a spatial resolution of 0.1° , forced by a corrected version of the ARPERA winds at 0.5° resolution, is run for the 42-year period 1960–2001 to produce wave parameters over the Hellenic Seas every 6 h. Wave height and direction are evaluated for their validity through comparison with in situ and space-born observations and after certain adjustments they are analysed to assess the wave climate of the Hellenic Seas.

The validation of the WAM model output revealed a good agreement with in situ and satellite observations at offshore locations characterised by a relatively simple topography in the main fetch direction. In the opposite case, a fair agreement was obtained, which was however often impaired for extreme wave heights. Specifically, the extreme SWH in the Aegean Sea, particularly its southern half, was considerably overestimated in the model hindcast. As a result, the original model SWH hindcast was adjusted. The adjusted model hindcast was found to perform reasonably well in the extreme SWH range and it was thus used in the computation of the extreme wave climate statistics. On the other hand, the original model hindcast was found to be preferable for the computation of the mean wave climate of the Hellenic Seas. Although the presented wave climate statistics are expected to fairly represent reality, nearshore values should still be

interpreted with caution because of errors associated with the resolution of the wind and wave models and because of increased uncertainty—due to a lack of observational data—in the derivation of the adjustment coefficients used to obtain the adjusted model hindcast.

The results of this work on the wave climate of the Hellenic Seas show that the mean wave climate acquires its maximum values in the vicinity of the straits west and east of the island of Crete, outside the Aegean Sea. In agreement, Chronis et al. (2011) refer to the presence of wind ‘lobes’ of high intensity to west and east of Crete corresponding to the respective exiting points of the northerly air flow in the Aegean Sea which is characterised by consistently the highest sustained magnitudes over the entire Mediterranean. High values are also observed in the Aegean Sea except for its northern part. The extreme wave climate acquires its maximum values principally in the southeastern Ionian Sea. High values also exist about the exits of the Aegean Sea, SE of Crete and N-NE of the Cyclades complex and the island of Euboea. As explained in Kotroni et al. (2001), the topographic particularities of the Aegean Sea such as wind funnelling through the numerous islands present can enhance the presence of extreme wind events; in turn, of extreme wave events. This results in a typical wave height range that is similar to the one observed in the Ionian Sea despite the shorter fetches characterising the Aegean Sea. In summer in particular, the magnitude of the extreme wave heights in the Ionian and Aegean Seas is comparable, whilst the maximum values are observed around the exits of the Aegean Sea into the Levantine Sea and to the S-SE. Nevertheless, the year-long most intense sea states are found in the Ionian Sea because of the long fetch distance. These are typically of a shorter duration than those found in the Aegean Sea which may be attributed to the aforementioned persistence of the northerly air flow within the later basin.

The computation of SWH return levels shows that different estimation methods result in return levels that do not present statistically significant differences when applied to the Hellenic Seas. Also, they result in very similar spatial patterns despite differences in absolute values. Nevertheless, the latter can substantially deviate when return periods of more than 100 years are considered.

The estimation of long-term SWH trends demonstrates statistically significant decreasing trends in both the mean (-0.3 cm/year) and extreme (-1.4 cm/year) wave conditions as well as in the average intensity of extreme events (-2.5 cm/year). Increasing trends are present in the Aegean Sea for the 99th-ile SWH and the average intensity of extreme events, but these are statistically insignificant. Seasonally, statistically significant decreasing trends are present in both winter and summer whilst spring and autumn are mainly characterised by insignificant increase. It is found that the aforementioned tendencies are not characteristic of the entire 1960–2001 period. A turning point is located around the year 1981 with the mean

and extreme wave climate increasing to this year and decreasing afterwards. A persistent decrease before and after 1981 is found in the Aegean Sea for the mean SWH but this is statistically insignificant.

The comparison of the extreme wave climate statistics computed with the adjusted model hindcast against those computed with the original model hindcast showed that absolute SWH differences between the two did not exceed 1 m but in the southern Aegean Sea, along the east coast of the mainland Greece and in the Gulf of Patras. The largest differences of up to about 3 m were obtained for parameters such as the maximum SWH and the 100-year SWH return level. The differences did not exceed 0.4 m for the average intensity of extreme events. Relatively small differences of up to 1.6 m were found for the long-term 99th-ile; these were largely confined within the SE Cyclades complex. Small differences were also obtained with respects to the magnitude of the SWH climatic trends. Storm characteristics such as the average number of peaks and the average storm duration were not affected by definition. The same is true for the distribution and statistical significance of the climatic trend slopes. This comparison gives us an insight on the bias expected in the estimation of extreme wave climate statistics given the performance statistics of the original hindcast. In addition, the similarity of the results in most of the examined domain before and after the model hindcast adjustment provides us with extra confidence on the results of this study on the extreme wave climate of the Hellenic Seas.

It is the first time that an in-depth analysis of the extreme wave climate of the Hellenic Seas and its trends is performed, along with the estimation of various engineering parameters like the storm frequency, intensity and duration as well as the SWH return levels. This information is valuable to the offshore and coastal engineer and is extremely relevant to the Hellenic Seas since this is a region characterised by intense offshore and coastal activity. As a next step, to assure sound long-term marine planning, it is important to determine whether the estimated wave climate and its trends are expected to remain unchanged in the future under the influence of climate change.

Acknowledgements This work has been supported by the MEDESS-4MS EU INTERREG MED project. We are grateful to Dr. S. Somnot for providing the atmospheric forcing dataset through the SESAME project. The calibration of the atmospheric dataset was done for the needs of the MEDECOS (MarinERA EU FP6) project. We thank George Krokos for his overall help with the atmospheric dataset. Finally, we also thank Dr. P. Queffeuilou for his valuable help on the satellite dataset and its proper use.

References

- Appendini CM, Torres-Freyermuth A, Salles P et al (2014) Wave climate and trends for the Gulf of Mexico: a 30-yr wave hindcast. *J Clim* 27: 1619–1632. doi:10.1175/JCLI-D-13-00206.1

- Athanassoulis GA, Skarsoulis EK (1992) Wave and wind Atlas of the North-Eastern Mediterranean Sea. Monogr. Natl. Tech. Univ. Athens Hell. Navy
- Caires S (2009) A comparative simulation study of the annual maxima and the peaks-over-threshold methods. Deltares report 1200264-002
- Caires S, Sterl A (2005) A new nonparametric method to correct model data: application to significant wave height from the ERA-40 Re-analysis. *J Atmos Ocean Technol* 22:443–459
- Cavaleri L, Bertotti L (2004) Accuracy of the modelled wind and wave fields in enclosed seas. *Tellus A* 56:167–175. doi:10.3402/tellusa.v56i2.14398
- Cavaleri L, Sclavo M (2006) The calibration of wind and wave model data in the Mediterranean Sea. *Coast Eng* 53:613–627. doi:10.1016/j.coastaleng.2005.12.006
- Chronis T, Papadopoulos V, Nikolopoulos EI (2011) QuickSCAT observations of extreme wind events over the Mediterranean and Black Seas during 2000–2008. *Int J Climatol* 31:2068–2077. doi:10.1002/joc.2213
- Coles S (2001) An introduction to statistical modeling on extreme values. Springer
- Debernard JB, Røed LP (2008) Future wind, wave and storm surge climate in the Northern Seas: a revisit. *Tellus A* 60:427–438. doi:10.1111/j.1600-0870.2008.00312.x
- Gulev SK, Grigorieva V, Sterl A, Woolf D (2003) Assessment of the reliability of wave observations from voluntary observing ships: insights from the validation of a global wind wave climatology based on voluntary observing ship data. *J Geophys Res* 108:1–21. doi:10.1029/2002JC001437
- Günther H, Hasselman S, Jansen PAEM (1992) The WAM model cycle 4. Tech. Rep. 4, DKRZ
- Herrmann MJ, Somot S (2008) Relevance of ERA40 dynamical downscaling for modeling deep convection in the Mediterranean Sea. *Geophys Res Lett* 35:1–5. doi:10.1029/2007GL032669
- Korres G, Papadopoulos A, Katsafados P et al (2011) A 2-year intercomparison of the WAM-Cycle4 and the WAVEWATCH-III wave models implemented within the Mediterranean Sea. *Mediterr Mar Sci* 12:129–152
- Kotroni V, Lagouvardos K, Lalas D (2001) The effect of the island of Crete on the Etesian winds over the Aegean Sea. *Q J R Meteorol Soc* 127:1917–1937. doi:10.1002/qj.49712757604
- Krokos G, Korres G (2010) Evaluation and corrections of air sea fluxes of a dynamical downscaled version of ERA40 reanalysis dataset for the Mediterranean Sea. In: The significance of marine science and the role of marine scientists in present-day Europe. European Federation of Marine Science and Technology (EFMS), Athens, Greece
- Lionello P, Sanna A (2005) Mediterranean wave climate variability and its links with NAO and Indian Monsoon. *Clim Dyn* 25:611–623. doi:10.1007/s00382-005-0025-4
- Lionello P, Rizzoli PM, Boscolo R (2006) Mediterranean climate variability, developments in earth and environmental sciences. Elsevier
- Martínez-Asensio A, Marcos M, Jordà G, Gomis D (2013) Calibration of a new wind-wave hindcast in the Western Mediterranean. *J Mar Syst* 121–122:1–10. doi:10.1016/j.jmarsys.2013.04.006
- Martucci G, Carniel S, Chiggiato J et al (2010) Statistical trend analysis and extreme distribution of significant wave height from 1958 to 1999—an application to the Italian Seas. *Ocean Sci* 6:525–538. doi:10.5194/os-6-525-2010
- Medatlas Group (2004) Wind and Wave Atlas of the Mediterranean Sea. West Eur Union
- Musić S, Nicković S (2008) 44-year wave hindcast for the Eastern Mediterranean. *Coast Eng* 55:872–880. doi:10.1016/j.coastaleng.2008.02.024
- NGDC (2006) 2-minute Gridded Global Relief Data (ETOPO2v2). In: Natl. Ocean. Atmos. Admin., U. S. Dept. Commer. <http://www.ngdc.noaa.gov/mgg/fliers/06mgg01.html>
- Nittis K, Perivoliotis L, Korres G, et al (2010) POSEIDON II: Upgrading the monitoring and forecasting services in the Eastern Mediterranean Sea. In: Dahlin H, et al (eds) *Coast. to Glob. Oper. Oceanogr. Achiev. Challenges. Proc. 5th Int. Conf. EuroGOOS 20-22 May, 2008*. Exeter, UK, pp 392–398
- Poupkou A, Zanis P, Nastos P et al (2011) Present climate trend analysis of the Etesian winds in the Aegean Sea. *Theor Appl Climatol* 106:459–472. doi:10.1007/s00704-011-0443-7
- Queffelec P, Bentamy A (2007) Analysis of wave height variability using altimeter measurements: application to the Mediterranean Sea. *J Atmos Ocean Technol* 24:2078–2092. doi:10.1175/2007JTECH0507.1
- Queffelec P, Croizé-Fillon D (2013) Global altimeter SWH data set—May 2013. Technical Report. URL <ftp://ftp.ifremer.fr/ifremer/cersat/products/swath/altimeters/waves/documentation/>
- Ratsimandresy AW, Sotillo MG, Carretero Albiach JC et al (2008) A 44-year high-resolution ocean and atmospheric hindcast for the Mediterranean Basin developed within the HIPOCAS Project. *Coast Eng* 55:827–842. doi:10.1016/j.coastaleng.2008.02.025
- Ruti PM, Marullo S, D’Ortenzio F, Tremant M (2008) Comparison of analyzed and measured wind speeds in the perspective of oceanic simulations over the Mediterranean basin: analyses, QuickSCAT and buoy data. *J Mar Syst* 70:33–48. doi:10.1016/j.jmarsys.2007.02.026
- Soukissian T, Prospathopoulos A, Hatzinaki M, Kabouridou M (2008) Assessment of the wind and wave climate of the Hellenic Seas using 10-year hindcast results. *Open Ocean Eng J* 1–12
- Uppala SM, Kållberg PW, Simmons AJ et al (2005) The ERA-40 reanalysis. *Q J R Meteorol Soc* 131:2961–3012. doi:10.1256/qj.04.176
- Van der Westhuysen AJ, van Dongeren AR, Groeneweg J et al (2012) Improvements in spectral wave modeling in tidal inlet seas. *J Geophys Res* 117:C00J28. doi:10.1029/2011JC007837
- WAMDI Group (1988) The WAM model—a third generation ocean wave prediction model. *J Phys Oceanogr* 18:1775–1810. doi:10.1175/1520-0485(1988)018<1775:TWMTGO>2.0.CO;2
- WASA Group (1998) Changing waves and storms in the Northeast Atlantic? *Bull Am Meteorol Soc* 79:741–760
- Weisse R, Günther H (2007) Wave climate and long-term changes for the Southern North Sea obtained from a high-resolution hindcast 1958–2002. *Ocean Dyn* 57:161–172. doi:10.1007/s10236-006-0094-x